Biochimica et Biophysica Acta 1840 (2014) 2730–2743

Contents lists available at ScienceDirect

Biochimica et Biophysica Acta

journal homepage: www.elsevier.com/locate/bbagen

Combinatorial anticancer effects of curcumin and 5-fluorouracil loaded thiolated chitosan nanoparticles towards colon cancer treatment

A. Anitha, N. Deepa, K.P. Chennazhi, Vinoth-Kumar Lakshmanan, R. Jayakumar *

Amrita Centre for Nanosciences and Molecular Medicine, Amrita Institute of Medical Sciences and Research Centre, Amrita Vishwa Vidyapeetham University, Kochi 682041, India

ARTICLE INFO

Article history:
Received 24 March 2014
Received in revised form 22 May 2014
Accepted 9 June 2014
Available online 17 June 2014

Keywords:
Combinatorial nanomedicine
Colon cancer
Pharmacokinetics
Thiolated chitosan
5-Fluorouracil
Curcumin

ABSTRACT

Background: Evaluation of the combinatorial anticancer effects of curcumin/5-fluorouracil loaded thiolated chitosan nanoparticles (CRC-TCS-NPs/5-FU-TCS-NPs) on colon cancer cells and the analysis of pharmacokinetics and biodistribution of CRC-TCS-NPs/5-FU-TCS-NPs in a mouse model.
Methods: CRC-TCS-NPs/5-FU-TCS-NPs were developed by ionic cross-linking. The in vitro combinatorial anticancer effect of the nanomedicine was proven by different assays. Further the pharmacokinetics and biodistribution analyses were performed in Swiss Albino mouse using HPLC.
Results: The 5-FU-TCS-NPs (size: 150 ± 40 nm, zeta potential: +48.2 ± 5 mV) and CRC-TCS-NPs (size: 150 ± 20 nm, zeta potential: +35.7 ± 3 mV) were proven to be compatible with blood. The in vitro drug release studies at pH 4.5 and 7.4 showed a sustained release profile over a period of 4 days, where both the systems exhibited a higher release in acidic pH. The in vitro combinatorial anticancer effects in colon cancer (HT29) cells using MTT, live/dead, mitochondrial membrane potential and cell cycle analysis measurements confirmed the enhanced anticancer effects (2.5 to 3 fold). The pharmacokinetic studies confirmed the improved plasma concentrations of 5-FU and CRC up to 72 h, unlike bare CRC and 5-FU.
Conclusions: To conclude, the combination of 5-FU-TCS-NPs and CRC-TCS-NPs showed enhanced anticancer effects on colon cancer cells in vitro and improved the bioavailability of the drugs in vivo.
General significance: The enhanced anticancer effects of combinatorial nanomedicine are advantageous in terms of reduction in the dosage of 5-FU, thereby improving the chemotherapeutic efficacy and patient compliance of colorectal cancer cases.

1. Introduction

Colorectal cancer constitutes about 40% of cancers diagnosed yearly and is the third most leading cause of mortality among cancer patients (lung, female breast, colorectal and stomach cancers) [1,2]. 5-FU, a chemo drug used against colon cancer acts by inhibiting the S phase of the cell cycle, thereby blocking the synthesis of DNA, and triggering cell death [3–9]. Chemotherapy using 5-FU has a major limitation in relation to non-specificity [10,11] and moreover 5-FU is resistant to colon cancer [12]. Literatures suggest that the effectiveness of 5-FU as a chemo drug in colon cancer treatment could be improved by combinatorial approach, wherein either conventional chemo drugs [2] or other nontoxic plant derived materials such as genistein [13,14], geraniol [13,14], and curcumin, CRC, [15,16] were used. The combinatorial approach with CRC makes it more important because of its well proven anticancer potential towards many cancers [16–19] and its safety in preclinical/clinical trials [20]. In colon cancer, CRC induces anticancer effects through multiple mechanisms [21].

Even though CRC has wide potential as a chemotherapeutic agent, the usage is limited due to its low bioavailability [22] which is a result of rapid metabolism [22] and the inactive metabolites [22]. Bioavailability of CRC could be enhanced either by absorption enhancers such as piperine [23] or encapsulating the drug CRC in nano, as well as microparticle system made from different polymeric carrier systems [23–27]. The combinatorial anticancer effects of 5-FU with CRC has been proven, the challenges being toxicity and low bioavailability

Abbreviations: 5-FU, 5-fluorouracil; CRC, curcumin; TCS, thiolated chitosan; FT-IR, Fourier transform infrared spectroscopy; DDA, degree of deacetylation; DLS, dynamic light scattering; PBS, phosphate buffered saline; SEM, scanning electron microscope; FBS, fetal bovine serum; RPM I, Roswell Park Memorial Institute medium; HPLC, high pressure liquid chromatography; EPR, enhanced permeability and retention effect; NPs, nanoparticles; BSA, bovine serum albumin; 5-FU-TCS-NPs, 5-fluorouracil loaded thiolated chitosan nanoparticles; CRC-TCS-NPs, curcumin loaded thiolated chitosan nanoparticles; MTT, [3-(4,5-dimethylthiazol-2-yl)-2,5-diphenyl tetrazolium bromide]; Rh 123, rhodamine 123; PI, propidium iodide; RNase, ribonuclease; Hb, hemoglobin; PT, prothrombin time; aPTT, activated partial thromboplastin time; PPP, platelet poor plasma; Mw, molecular weight; TPP, pentasodium tripolyphosphate; CO_2, carbon dioxide; EDTA, ethylene diamine tetra acetic acid; OD, optical density; JC-1, 5,5′,6,6′-tetraethylbenzidazolylcarbocyanine iodide; AUC, area under the curve; ACD, acid citrate dextrose; H and E, Harris's Hematoxylin and Eosin; FdUMP, fluorodeoxyuridine monophosphate; FdUTP, fluorodeoxyuridine triphosphate; FUTP, fluorouridine triphosphate; DNA, deoxyribonucleic acid; RNA, ribonucleic acid; COX-2, cyclooxygenase-2; pH, potenz hydrogen; HT29, human colon adenocarcinoma; IEC 6, mouse intestinal epithelial cells

* Corresponding author. Tel.: +91 484 2801234; fax: +91 484 2802020.
E-mail addresses: rjayakumar@aims.amrita.edu, jayakumar77@yahoo.com (R. Jayakumar).

http://dx.doi.org/10.1016/j.bbagen.2014.06.004
0304-4165/

respectively. Nanoencapsulation technique is widely used for entrapping diverse drugs, and in a way advantageous as it increases the bioavailability of CRC and 5-FU [5,25,28]. In addition, the nanosized particles help in more tumor accumulation because of their enhanced permeability and retention effect (EPR) [25]. There have been several reports suggesting the potential of CRC as a suitable replacement for genistein and geraniol and it was shown to promote the efficacy of 5-FU in various cancers including colon cancer [14,28]. The augmented combinatorial antitumorigenic potential of CRC with 5-FU towards colon cancer has already been reported [13,14,28]. The mechanism of combinatorial effect involves the inhibition of cyclooxygenase-2 (COX-2) in the mRNA and protein levels, which is overexpressed in many kinds of colon cancers [13,14,28].

The current thesis work focuses on an effective strategy to improve the efficacy of 5-FU assisted chemotherapy against colon cancer. This has been addressed by combinatorial approach in which CRC was used in combination with 5-FU. The potential of both drugs was improved by nanoencapsulation, wherein a non-toxic polymeric carrier system; 'thiolated chitosan' (TCS) [29,30] was used. Thus the developed 5-FU-loaded-thiolated chitosan nanoparticles (5-FU-TCS-NPs) and CRC-loaded-thiolated chitosan nanoparticles (CRC-TCS-NPs) were characterized, and evaluated for their in vitro combinatorial anticancer effects and in vivo plasma concentration–time profile.

2. Materials and methods

2.1. Materials

Chitosan (Mw: 100–150 kDa and DDA—80%) was purchased from Koyo Chemical Co Ltd., Japan, TCS (degree of thiol substitution: 60 ± 6%) was prepared based on the reported literatures [29,30]. 5-FU, CRC, BSA, pentasodium tripolyphosphate (TPP), dialysis tubings (Mw cut-off 12 kDa), Triton X-100, MTT [3-(4,5-dimethylthiazol-2-yl)-2,5-diphenyl tetrazolium bromide], rhodamine 123 (Rh 123), propidium iodide (PI) and RNase were purchased from Sigma Aldrich. Colon cancer (HT29) and mouse intestinal epithelial cells (IEC 6) were purchased from NCCS Pune, India. A mitochondrial membrane potential assay kit was purchased from Invitrogen and all other chemicals used are of analytical grade and used without further purification.

2.2. Synthesis of 5-FU-TCS-NPs

5-FU was dissolved in methanol (1 mg/ml) and it was incubated with TCS solution, 45 ml (22.5 mg of TCS and 5 mg of 5-FU) overnight. Further the drug incubated TCS samples were cross-linked with TPP (1%) solution for a volume ratio of (TCS:TPP, 45:1), followed by incubating with 0.1 ml of 1% BSA solution for 30 min. The drug loaded-nanoparticles were separated from the suspension by centrifugation at 15,000 rpm for 30 min. The supernatant was discarded and the pellet was redispersed in saline and it was used for further characterization and studies.

2.3. Synthesis of CRC-TCS-NPs

CRC incorporated TCS solutions [CRC in ethanol, 1 mg/ml for a ratio of 45 ml (22.5 mg of TCS, 5 mg of CRC)] was cross-linked with TPP (1%) followed by incubating with 0.1 ml of 1% BSA solution for 30 min. The drug loaded-nanoparticles were separated by centrifugation (15,000 rpm for 30 min). The resulting supernatant and pellet were collected and were used for further characterization and studies.

2.4. Labeling of Rh 123 to CRC-TCS-NPs and 5-FU-TCS-NPs

Rh 123 was labeled to the CRC-TCS-NPs and 5-FU-TCS-NPs using ionic interaction and physical adsorption. The redispersed nanoparticle pellet of 5-FU-TCS-NPs and CRC-TCS-NPs was separately incubated with Rh 123 (5 mg/ml, 0.5 ml) overnight and stirred in the dark. The resulting Rh 123 labeled nanoparticles were centrifuged (15,000 rpm for 15 min), and washed (3 times with water). The washed pellet was redispersed in saline and was used for cellular uptake studies.

2.5. Entrapment efficiency (EE) and loading efficiency (LE) of 5-FU-TCS NPs and CRC-TCS-NPs

The EE and LE of the 5-FU-TCS-NPs/CRC-TCS-NPs were quantified using spectrophotometry [31,32]. For this, the drug loaded-nanoparticle pellets of 5-FU-TCS-NPs and CRC-TCS-NPs were separated from the nanoparticle suspension by centrifugation (15,000 rpm for 30 min), lyophilized, and weighed. The lyophilized drug loaded-nanoparticles of 5-FU-TCS-NPs and CRC-TCS-NPs were used for extracting the entrapped 5-FU and CRC. The extraction procedure is explained below. For the CRC-TCS-NPs, the lyophilized pellets were treated with ethanol to completely redissolve the entrapped CRC (vortexing, and probe sonication) and centrifuged. The yellowish supernatant was collected, and the absorbance value was measured using a spectrophotometer at 429 nm. The corresponding drug concentration was calculated from the calibration graph of CRC. Similarly for the 5-FU-TCS-NPs, the lyophilized 5-FU-TCS-NP pellet was treated with methanol to completely redissolve the entrapped 5-FU (vortexing, and probe sonication), centrifuged, and the supernatant was collected. The absorbance value was measured using a UV–vis spectrophotometer at 262 nm. The corresponding drug concentration was calculated from the calibration graphs of 5-FU. The EE and LE of the 5-FU-TCS-NPs/CRC-TCS-NPs can be calculated using the following equations:

$$\mathrm{EE}(\%) = \frac{\text{Amount of entrapped drug(CRC or FU)present in the pellet}}{\text{Initial amount of 5-FU or CRC used for the drug encapsulation}} \times 100$$

$$\mathrm{LE}(\%) = \frac{\text{Amount of entrapped drug(CRC or FU)present in the pellet}}{\text{Weight of the lyophilized CRC-TCS-NPs/5-FU-TCS-NPs(yield)}} \times 100.$$

2.6. Characterizations of 5-FU-TCS-NPs and CRC-TCS-NPs using DLS, SEM, zeta potential and FT-IR

The particle size of the developed nanoparticle was measured using DLS (DLS-ZP/Particle Sizer Nicomp™ 380 ZLS) and SEM (JEOLJSM-6490LA). Stability was analyzed using zeta potential measurements (Zeta sizer, DLS-ZP/Particle Sizer Nicomp™ 380 ZLS). Fourier transform infrared spectroscopy (FT-IR) was used to analyze the potential chemical interaction between the TCS and the drugs (Perkin Elmer Spectrum RXI Fourier Transform Infrared spectrophotometer).

2.7. Drug release studies

The in vitro release profile of 5-FU from 5-FU-TCS-NPs and CRC from CRC-TCS-NPs was carried out based on the reported protocols [31,32] using dialysis, for 5-FU [32] and the Eppendorf method for CRC [31] and the studies were carried out at pH 4.5 and 7.4 at 37 °C under sink conditions [31]. The protocol for 5-FU release is explained as follows. The drug loaded-nanoparticle pellet was redispersed in 3 ml water, mixed homogeneously and transferred to dialysis tubes. The dialysis tubing containing nanoparticle sample was kept in a beaker containing phosphate buffered saline (PBS) at pH 7.4 and 4.5 separately. The resulting system was incubated in a water bath shaker at 37 °C under shaking. At predetermined time intervals, 0.75 ml of release media was taken from the beaker and replenished with fresh PBS. The released drug in PBS was measured using a spectrophotometer at 262 nm. This was continued for 4 days and the released drug at each time point was quantified using calibration graphs.

For the CRC release, the CRC-TCS-NP pellet was redispersed in a measured volume of PBS of pH 4.5 and 7.4. The resulting NPs were homogeneously mixed and divided into 0.5 ml volumes in different Eppendorf tubes. The samples in the Eppendorf tubes were incubated in a water bath shaker at 37 °C. At different time intervals, triplicate samples were taken out; an equal amount of ethanol was added to redissolve the released CRC, centrifuged at 5000 rpm for 10 min, and the supernatant was collected and analyzed for the amount of released CRC at 429 nm using a spectrophotometer. The drug concentrations were calculated using the calibration graphs. The two experiments were repeated thrice to verify the data. The drug release percentage was calculated using the following formula.

$$\text{Release}(\%) = \frac{\text{Concentration of released drug at each time point}}{\text{Concentration of entrapped drug within the NPs}} \times 100.$$

2.8. In vitro blood compatibility studies

Blood compatibility was assessed using hemolysis and coagulation time measurements, wherein the former experiments prove the non-destroying potential of the prepared nanoparticles towards red blood cells (RBC) and the latter confirm the non-clotting nature of the nanoparticles towards blood. Both experiments were done based on the reported protocols [31,32] for a range of concentration (10–80 μM of drug loaded-TCS NPs).

2.9. Hemolysis assay of 5-FU-TCS-NPs and CRC-TCS-NPs

The hemolysis assay involves the incubation of blood (0.9 ml) with nanoparticle samples (0.1 ml) at 37 °C for 3 h followed by measuring the percentage of plasma hemoglobin by absorbance measurements. The controls include Triton X (1%) and saline-treated (1%) blood as positive and negative controls, respectively. Plasma hemoglobin concentration was calculated based on the following equation.

$$\text{Plasma Hb} = \frac{[(2A_{415}) - (A_{380} + A_{450})] \times 1000 \times \text{Dilution factor}}{E \times 1.655}$$

where A_{415}, A_{380} and A_{450} are the absorbance values at 415, 380 and 450 nm. A_{415} is the absorption band of hemoglobin. A_{380} and A_{450} are correction factors applied for uroporphyrin absorption falling in the same wavelength range. E is the molar absorptivity value of oxyhemoglobin at 415 nm which is 79.46 and 1.655 is the correction factor which accounts for the turbidity of the plasma sample. The percentage hemolysis was obtained using the following formula.

$$\text{Hemolysis}(\%) = \frac{\text{Plasma Hb value of sample}}{\text{Total Hb of blood}} \times 100.$$

2.10. Coagulation assay: PT and aPTT measurements

The exposure of nanoparticles to blood can induce coagulation cascade. In order to evaluate the effect of the prepared CRC-TCS-NPs and 5-FU-TCS-NPs towards the blood coagulation cascade, a coagulation assay has been carried out. The assay was done using prothrombin time (PT) and activated partial thromboplastin time (aPTT) measurements. The protocol involves the separation of platelet poor plasma (PPP) from blood (by centrifuging the blood at 5000 rpm for 20 min) followed by incubating the PPP (0.9 ml) with different concentrations of 0.1 ml of CRC-TCS-NP/5-FU-TCS-NP samples and kept for 30 min of incubation at 37 °C. The treated PPP was used for measuring the PT and aPTT using the coagulation analyzer and reagent kits (CK Prest and Fibriprest from Diagnostica Stago (France)). The whole experiment was repeated thrice and in each case, triplicate samples were analyzed to confirm the data using saline treated-PPP as the negative control.

2.11. Cell culture

HT29 and IEC 6 cells were maintained in CO_2 incubators with 5% CO_2 at 37 °C in RPMI media (with 10% FBS and 100 units/ml of antibiotic). Once the cells reached 90% confluence, the cells were detached from the flask with trypsin-EDTA and the cell pellet was centrifuged at 1500 rpm for 3 min. Further the cell pellet was resuspended in complete media, counted using a hemocytometer and used for further cell culture experiments.

2.11.1. MTT assay: cytocompatibility of TCS nanoparticles

The cytocompatibility of the carrier system was proven by MTT assay for a range of concentration (0.2 to 2 mg/ml) in HT29 and IEC 6 cells for 48 h and the protocol followed was from our own earlier reports [30–32]. The underlying principle of MTT involves the reduction of tetrazolium component of MTT into purple colored formazan crystals by the mitochondrial reductase enzymes of viable cells. The formazan crystals produced have an absorption maximum of 570 nm. So the percentage of viable cells or viability can be quantified using the OD values at 570 nm. The OD values were measured using a Beckmann Coulter Elisa plate reader, BioTek Power Wave XS.

The cells were seeded in 24 well plates with a seeding density of 37,500 cells/well and kept for 24 h of incubation. Further the cells were incubated with 100 μl of nanoparticle samples in media for 48 h and MTT assay was performed. The experiment was done in triplicates and the entire experiment was done thrice using Triton-X 100 (1%) treated cells as negative control and normal tissue cultured wells as the positive control.

$$\text{Cell viability}(\%) = \frac{\text{Absorbance of the cells treated with the samples}}{\text{Absorbance of the untreated cells}} \times 100.$$

2.11.2. Cellular uptake studies using confocal microscopy

For microscopy experiments, cells were seeded in acid etched cover slips kept in 12 well plates with a density of 75,000 cells/cover slip. After 24 h, the cells were incubated with Rh 123 labeled nanoparticles for 6 h. After the incubation, cover slips were processed for imaging using a confocal microscope (Leica SP 5 II) to study the cellular internalization of Rh 123-5-FU-TCS-NPs and Rh-123-CRC-TCS-NPs.

2.11.3. In vitro combinatorial anticancer effects of CRC-TCS-NPs and 5-FU-TCS-NPs towards HT29 cells

The in vitro combinatorial anticancer effects of CRC-TCS-NPs and 5-FU-TCS-NPs were evaluated in HT29 cells in comparison with the individual drug loaded-nanoparticles and control bare drugs. The combinatorial anticancer effects were initially proved by scratch (cell migration), MTT, live/dead assays and further confirmed by mitochondrial membrane potential and cell cycle analysis measurements.

2.11.3.1. Cell migration assay. The migration ability of HT29 cells after the sample treatment was analyzed by migration or scratch assay. Here the scratches were made to the confluent cells and the closing of the scratch was analyzed using an optical microscope. HT29 cells were seeded with a density of 3×10^5 cells in 6 well plates, once a monolayer was formed, scratches were made with a pipette tip, washed with PBS, and microscopic images were taken. To the cells, samples of 5-FU-TCS-NPs (20 μM), CRC-TCS-NPs (20 μM), and the combination of NPs (5-FU-TCS-NPs and CRC-TCS-NPs, 20 μM) were added along with control bare drugs. The closure of the wound/scratch was observed in every 0 to 48 h with a Leica microscope and photographs were taken [33]. The wound area was measured before and after the sample treatments and the corresponding wound closure assay graphs were plotted.

2.11.3.2. MTT assay. For MTT assay, HT29 and IEC 6 cells were seeded onto a 24 well plate with a density of 37,500 cells per well and kept

for 24 h. After the incubation, samples with media were added individually and in combination to triplicate wells, and incubated for 48 h. The sample concentrations include 20 μM 5-FU, 20 μM CRC, combination of both, 20 μM CRC-TCS-NPs, 20 μM 5-FU-TCS-NPs, and a combination of 20 μM 5-FU-TCS-NPs/20 μM CRC-TCS-NPs and kept for 48 h of incubation and MTT assay was performed.

2.11.3.3. Live/dead assay. For the live/dead assay experiments, acid etched cover slips kept in 12 well plates were seeded with a density of 75,000 cells per well and kept for 24 h for attaching onto the cover slips. Further the cells were treated with the samples (20 μM 5-FU, 20 μM CRC, combination of both, 20 μM 5-FU-TCS-NPs, 20 μM CRC-TCS-NPs, combination of 20 μM 5-FU-TCS NPs and 20 μM CRC-TCS-NPs) and kept for 48 h of incubation. After the desired incubation period, the media was replaced with PBS containing dye mixtures (acridine orange and ethidium bromide; acridine orange stains live cells green while ethidium bromide stains dead cells red-to-orange), and incubated for 20 min. The cover slips were directly taken and viewed under the fluorescent microscope to visualize the fluorescence coming from live as well as dead cells. Further the cell death induced by the combination of CRC-TCS-NPs and 5-FU-TCS-NPs was quantified and confirmed using different experiments.

2.11.3.4. Mitochondrial membrane potential measurements ($\Delta\Psi m$). The mitochondrial membrane potential changes happening during cell death were measured using JC-1 (5,5′,6,6′-tetraethylbenzidazolylcarbocyanine iodide) assay. Polarized mitochondria in healthy live cells form JC-1 aggregates, whereas it remains as monomers in the mitochondria of dead or apoptotic cells. The JC-1 aggregates and monomers have fluorescence in the red and green regions respectively. Thus the changes in the mitochondrial membrane potential happening during apoptosis were measured using the emission from the JC-1 monomers and aggregates [20]. The experiments were carried out in 6 well plates with a seeding density of 1.5 lakh cells/well and incubated for 24 h. The cells were incubated with media containing samples (CRC-TCS-NPs and 5-FU-TCS-NPs in combination in comparison with individual nanoformulations and control bare drugs) for 48 h. After the incubation, medium was collected, washed with PBS, and the cells were trypsinized. The cell pellets were incubated with 0.5 ml of the JC-1 reagent solution in buffer at 37 °C for 15 min. The resulting samples were centrifuged at 5000 rpm for 5 min, washed with buffer, resuspended in the assay buffer and analyzed using a flow cytometer.

2.11.3.5. Cell cycle analysis. The combinatorial anticancer effects of CRC-TCS-NPs and 5-FU-TCS-NPs towards HT29 cells were further confirmed and quantified using cell cycle analysis. The basic principle involves the staining of PI dye to DNA through intercalation and measuring the intensity of PI emission using a flow cytometer. The resulting data describe the percentage of cells in each phase, since the DNA content of cells in G0/G1, G2/M and S phase is 2n, 2n–4n and 4n respectively. The cell cycle analysis experiments were carried out in 6 well plates with a density of 4.5×10^5 cells and incubated for 24 h. Further the cells were treated with samples containing media and kept for 48 h incubation. After the desired incubation, cells were trypsinized, centrifuged, washed with PBS and fixed using 70% ethanol in PBS and incubated overnight in ice. The overnight incubated samples were centrifuged, washed with PBS, resuspended in PBS, and incubated with RNase for 30 min at 37 °C. The RNase treated cells were stained with PI, and analyzed using the flow cytometer.

2.12. In vivo drug quantification using HPLC

The in vivo drug quantification experiments were carried out using HPLC (LC 2010A HT SHIMADZU) with C18 columns, Qualisil BDS C18 chromatography column (5 μm, 4.6 × 250 mm) and Luna 5 μm C18 column (Phenomenox) respectively for 5-FU and CRC. The calibration protocols were followed from the reported literatures for 5-FU [34] and CRC [35–37]. The calibration graphs of 5-FU standards were made with methanol from the lowest to the highest concentrations and was analyzed using HPLC (isocratic), with a mobile phase of methanol: water mixture (10:90, v/v). The flow rate of the system was adjusted to 1 ml/min and the retention time obtained was found to be 4.2 ± 0.8 s. For each concentration, the area under the curve (AUC) was measured; and calibration graphs were plotted. The calibration experiments were done in triplicates and the same experiment was repeated on different days. The calibration experiments of CRC standards were made in ethanol from the lowest to highest concentrations, and was analyzed via HPLC (gradient elution) with a mobile phase of acetonitrile and 5% acetic acid (75: 25, v/v). The flow rate of the system was adjusted to 1 ml/min and the retention time obtained was found to be 3 ± 0.5 s. The AUC versus concentration graphs were plotted and the corresponding equations were used for further drug quantification. The calibration graphs of 5-FU and CRC were plotted to get the linearity and regression equation. The Limit of Detection (LOD) and Limit of Quantitation (LOQ) of CRC and 5-FU were determined using calibration graphs. LOD and LOQ values were calculated as 3.3 σ/S and 10 σ/S, respectively, where S is the slope of the calibration curve and σ is the standard deviation of response. A linear relationship between the drug concentration and the AUC value was observed with an r^2 value of greater than 0.9. In addition, the low LOD and LOQ values indicated the good sensitivity of the proposed method [38,39].

2.12.1. In vivo studies in Swiss Albino mice

The animal experiments were conducted in Swiss Albino mice with prior approval by the Institutional Animal Ethical Committee AIMS Kochi (Ref. No. IAEC/2012/1/3). The experiments were carried out by trained technicians. The animals were maintained in the Animal House facility with free access to food and water. The pharmacokinetics and biodistribution studies were carried out for 72 h. Swiss Albino female mice of 4–5 months (25–30 g) were injected with the samples through the tail vein. The samples involves 5-FU-TCS-NPs (NPs containing 20 mg/kg of 5-FU), CRC-TCS-NPs (NPs containing 25 mg/kg of CRC), combination of CRC-TCS-NPs and 5-FU-TCS-NPs, bare CRC (25 mg/kg of CRC: 6.25 mg/ml of CRC was dissolved in distilled water containing Tween 20 (1% v/v), it was diluted 10 times in saline and was used for animal studies) and 5-FU (20 mg/kg of 5-FU: 5 mg/ml of 5-FU was prepared in water, it was diluted 10 times in saline and was used for animal studies) in combination, and control saline. Once the samples were administered, blood samples (50 μl) were collected after 0.25,1,6,12, 24, 48 and 72 h through the retro orbital sinus. After 72 h, the animals were euthanized by intramuscular injection of an overdose of ketamine and xylazine. The organs; brain, heart, lungs, kidney, liver and spleen samples were collected in both saline and formalin. The respective organs in saline and formalin were used for biodistribution and histopathology studies. The experiment was done with an 'n' value of 4 ($n = 4$).

2.12.2. Pharmacokinetic evaluation

For the pharmacokinetic studies, the blood samples collected in acid citrate dextrose (ACD) at each time point was centrifuged at 4000 rpm for 5 min. The plasma was collected and stored in −20 °C until analysis. For the HPLC quantification, a measured amount of plasma was treated with methanol (1:9) and kept in −20 °C overnight to precipitate out the proteins. The plasma was separated from the protein precipitated plasma samples by centrifugation at 4000 rpm for 15 min. The resulting plasma (20 μl) was used for quantifying the CRC and 5-FU [34–37]. The pharmacokinetic parameters such as the concentration maximum (C_{max}), time of maximum concentration (t_{max}), area under the curve (AUC_{0-t}), half life ($t_{1/2}$), volume of distribution (V_d), and clearance (CL) were determined using a recently published Microsoft add-in tool, PK Solver [40]. The in vivo PK modeling was done by considering the whole body as a single compartment and AUC was calculated using the linear trapezoidal rule [40].

2.12.3. Biodistribution analysis

The organs collected in saline were dried in blotting paper and weighed. To the weighed organs, 1 ml of saline was added and homogenized using a tissue homogenizer. The homogenisate was treated with 1 ml of methanol overnight to redissolve the drugs. The resulting samples were centrifuged at 2000 rpm for 5 min. The supernatant was collected and analyzed using HPLC.

2.12.4. Histological analysis

The formalin fixed organs were grossed, kept in tissue cassettes and was processed in different grades of isopropyl alcohol and xylene. The processed tissues were embedded in paraffin wax and sections were taken with a thickness of 5 μm. The corresponding sections were stained with Harris's Hematoxylin–Eosin (H and E) reagent for histological observations under a light microscope [41].

2.13. Statistical analysis

All the in vitro experiments were done in triplicates and each experiment was repeated thrice to validate the data. The in vivo experiments were done with an 'n' value of 4. All the results were analyzed using Student t test as the statistical method and a 'p' value of <0.05 was considered to be significant.

3. Results

3.1. Synthesis of CRC-TCS-NPs and 5-FU-TCS-NPs

CRC-TCS-NPs and 5-FU-TCS-NPs were synthesized by ionotropic gelation utilizing TPP and the nanoparticle stabilization was enhanced by the addition of BSA [42]. The concentration of TCS was optimized to be 0.05% for a TPP concentration of 0.5% (ratio: 1:0.1). A stable nanoparticle system of 5-FU-TCS-NPs and CRC-TCS-NPs was obtained for a concentration of 5 mg of 5-FU and CRC. As the CRC concentration was increased above 10 mg, precipitation of drug happened, whereas for the 5-FU system, there is no enhancement in the entrapment efficiency. Hence, the above said optimized system was used for further analysis.

3.2. Characterization of CRC-TCS-NPs and 5-FU-TCS-NPs

3.2.1. Size characterization using DLS, SEM and stability studies using zeta potential measurements

The particle size distribution of CRC-TCS-NPs and 5-FU-TCS-NPs was confirmed using DLS (data not shown), and SEM. Fig. 1A and B represents the SEM images of 5-FU-TCS-NPs and CRC-TCS-NPs respectively. The characterization results confirmed the particle size as 150 ± 40 nm for 5-FU-TCS-NPs and 150 ± 20 nm for CRC-TCS-NPs. Apart from the size, SEM results proved the spherical morphology of the developed NPs. The zeta potential values were found to be +35.7 ± 3 and +48 ± 2 mV respectively for CRC-TCS-NPs and 5-FU-TCS-NPs (Table 1).

3.2.2. FT-IR spectral analysis: to study the interaction between the drugs and the TCS nanoparticles

FT-IR spectral analysis of CRC-TCS-NPs and 5-FU-TCS-NPs was carried out to study the potential chemical interaction between the TCS NPs, TPP and the drugs. Fig. 2(a), (b), (c), (d), (e) and (f) represents the FT-IR spectra of TCS NPs, BSA, CRC, CRC-TCS-NPs, 5-FU, and 5-FU-TCS-NPs respectively. TCS possesses its characteristic peaks in the regions (not shown), at 3410 (–O–H and –N–H stretching), 2924 (–C–H), 1623, 1513 (–N–H), 1088 (–C–N), 651 ($-NH_2$), 1380 (–C–H), 1248 (–O–H), 1153 (–C–O–C), 651 (due to amino groups) and 895 cm^{-1} (epimeric –C–H, of cyclic pyranosyl rings), 1524 (amide II band), 1629 (amide I band) and 1250 cm^{-1} peak corresponds to thiol groups. For the TCS NP spectrum, all the peaks of TCS were present, but most of the peak intensities were reduced (especially the 1637 peak, due to the ionic cross-linking reaction of TPP with the –N–H groups) [30,43,44]. The characteristic peak of 5-FU was found in the following regions, 3000–2900 cm^{-1} (–C–H stretching), 1425 cm^{-1} corresponding to the –C═N and –C═C ring stretching vibrations, and pyrimidine band at 1344 cm^{-1}. The absorption bands at 1180, 1639 and 1243 cm^{-1}

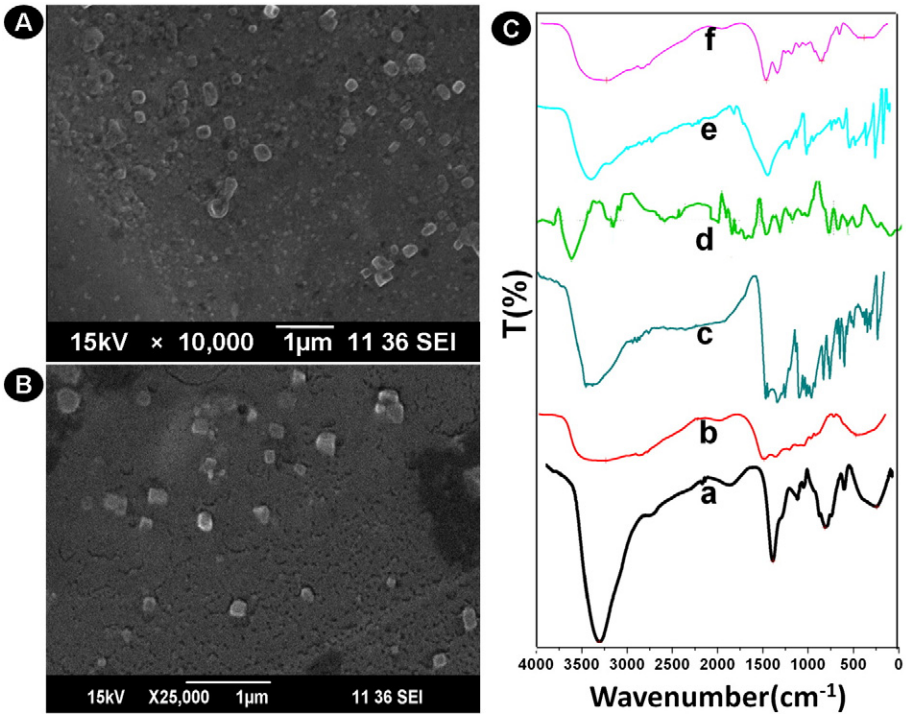

Fig. 1. (A) and (B) represent the size characterization data of 5-FU-TCS-NPs, and CRC-TCS-NPs, where (A) & (B) contain SEM images of 5-FU-TCS-NPs & CRC-TCS-NPs, and (C) FT-IR spectral analysis data, where (a) TCS NPs, (b) BSA,(c) CRC, (d) CRC-TCS-NPs, (e) 5-FU, and (f) 5-FU-TCS-NPs.

Table 1
Size, zeta potential, entrapment and loading efficiency values of 5-FU-TCS-NPs and CRC-TCS-NPs.

System	Size (nm)	Zeta potential (mV)	Entrapment efficiency (%)	Loading efficiency (%)
5-FU-TCS-NPs	150 ± 40	+48 ± 2	46.83 ± 3.2	16.55 ± 3.06
CRC-TCS-NPs	150 ± 20	+35.7 ± 3	85.53 ± 6.81	28.80 ± 3.89

were assigned to the –C–O and –C–N vibrations, respectively [32,45,46]. BSA possesses its characteristic peaks at 3430, 3062, 1652, and 1531 cm^{-1} respectively, due to the –OH stretching vibrations, amide A (–NH stretching), amide I (–NH stretching) and amide II (happens due to the coupling of bending vibration of –NH and stretching vibration of the –C–N bonds) [42]. In the spectrum of 5-FU-TCS-NPs, the characteristic peaks of 5-FU were present, but there was an enhancement in peak intensity and a shift in peak at 1630 cm^{-1} (TCS NPs) and 1639 cm^{-1} (5-FU). This was due to the formation of intermolecular hydrogen bonds between the –N–H groups of TCS NPs with the carbonyl and an F moiety of 5-FU [47,48]. CRC showed its characteristic absorption peaks in the range of 3510 cm^{-1} due to the phenolic –O–H stretching vibration. There were sharp absorption bands at 1605 cm^{-1} (stretching vibrations of benzene ring), 1502 cm^{-1} (–C═O and –C–C vibrations), 1435 cm^{-1} (olefinic –C–H bending vibration) and 1285 cm^{-1} (aromatic –C–O stretching vibration) [49,50]. Because of the entrapment of CRC in CRC-TCS-NPs, NP related peaks were shifted in the spectrum of CRC-TCS-NPs.

3.3. Entrapment efficiency (EE) and loading efficiency (LE)

The EE and LE of CRC-TCS-NPs and 5-FU-TCS-NPs were confirmed by spectrophotometry. The EE and LE of the systems were found to be 85.53 ± 6.81 & 28.8 ± 3.89 and 46.83 ± 3.2 & 16.55 ± 3.06% respectively for the CRC-TCS-NPs and 5-FU-TCS-NPs. As the CRC concentration was increased, the system tends to precipitate out the CRC. Whereas for the 5-FU-TCS-NPs, the increasing concentration of 5-FU during the synthesis results in low entrapment efficiency and the results are depicted in Table 1.

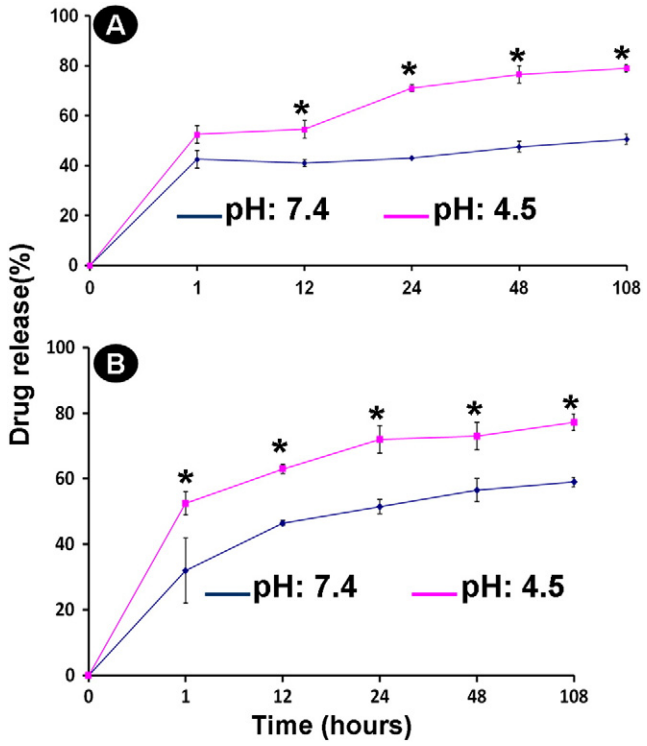

Fig. 2. In vitro drug release profile of CRC-TCS-NPs and 5-FU-TCS-NPs at pH 7.4 and 4.5 (done in triplicates; n = 3, and each experiment was repeated thrice, *$p < 0.05$, statistical significance).

3.4. In vitro drug release profile of CRC-TCS-NPs and 5-FU-TCS-NPs

The in vitro drug release results of 5-FU-TCS-NPs and CRC-TCS-NPs are depicted in Fig. 2, where (A) represents the release profile of CRC-TCS-NPs, and (B) represents the release profile of 5-FU-TCS-NPs. Both systems showed an initial burst release in both pHs, which results from the surface adsorbed drug. Later on, there was a sustained pattern that results from the slow degradation of the carrier matrix [32,50–52].

In Fig. 2A, it is clear that within the first 12 h, 40% CRC release occurred and up to 108 h, the percentage release stayed up to 42% (pH: 7.4), whereas in acidic pH an enhanced drug release was occurring. As a result, 80% of drug release happened within 108 h. For the 5-FU system, in pH 7.4, initial burst release was observed, which results in 30% release. As the time goes from the 12th to the 108th hour, the release was increased from 40 to 55%. In acidic pH, the release was enhanced which resulted in 65–70% release within 108 h.

3.5. Hemocompatibility of CRC-TCS-NPs and 5-FU TCS NPs: hemolysis and coagulation assays

The blood compatibility of 5-FU-TCS-NPs and CRC-TCS-NPs was confirmed using hemolysis and coagulation assays and the results were shown in Fig. 3. Fig. 3A depicts the hemolysis assay graph. In Fig. 3A, it is clear that the percentage hemolysis for all the samples treated with blood is below 5%. Fig. 3B shows the clotting assay graphs for a range of concentrations using PT and aPTT measurements. The PT and aPTT values of all the samples treated with PPP were in the normal range.

3.6. In vitro cytocompatibility of TCS NPs towards HT29 and IEC 6 cells

MTT assay results of the TCS NPs towards HT29 ad IEC 6 cells for a range of concentrations are shown in Fig. 3C (incubation time: 48 h). From the results, it was confirmed that the prepared TCS NPs were cytocompatible towards HT29 and IEC 6 cells for an incubation time of 48 h for concentrations ranging from 0.2 to 2 mg/ml.

3.7. In vitro cellular uptake studies of Rh 123-CRC TCS NPs and Rh 123-5-FU TCS NPs

The in vitro cellular uptake of Rh 123-CRC-TCS-NPs and Rh 123-5-FU-TCS-NPs by confocal imaging is shown in Fig. 4. The figure represents the confocal images of IEC 6 and HT29 cells treated with nanoparticle samples for 6 h. Fig. 4(a, a1), (d, d1) represents control IEC 6 and HT29 cells, Fig. 4(b, b1), (e, e1) represents the confocal images of cells treated with Rh 123-CRC-TCS-NPs samples and Fig. 4(c, c1), (d, d1) represents the confocal images of cells treated with the Rh 123-5-FU-TCS-NP samples. Panels a, b, c, d, e, f, g and a1, b1, c1, d1, e1, f1, g1 represent the bright and fluorescent images respectively. From the images it was proved that the cells which were incubated with nanoparticle samples showed intense green fluorescence of Rh 123 labeled NPs.

3.8. In vitro anticancer evaluation

The in vitro combinatorial anticancer effects of the CRC-TCS-NPs and 5-FU-TCS-NPs were evaluated using wound closure, MTT and live/dead assay and it was further confirmed by measuring the percentage of cell

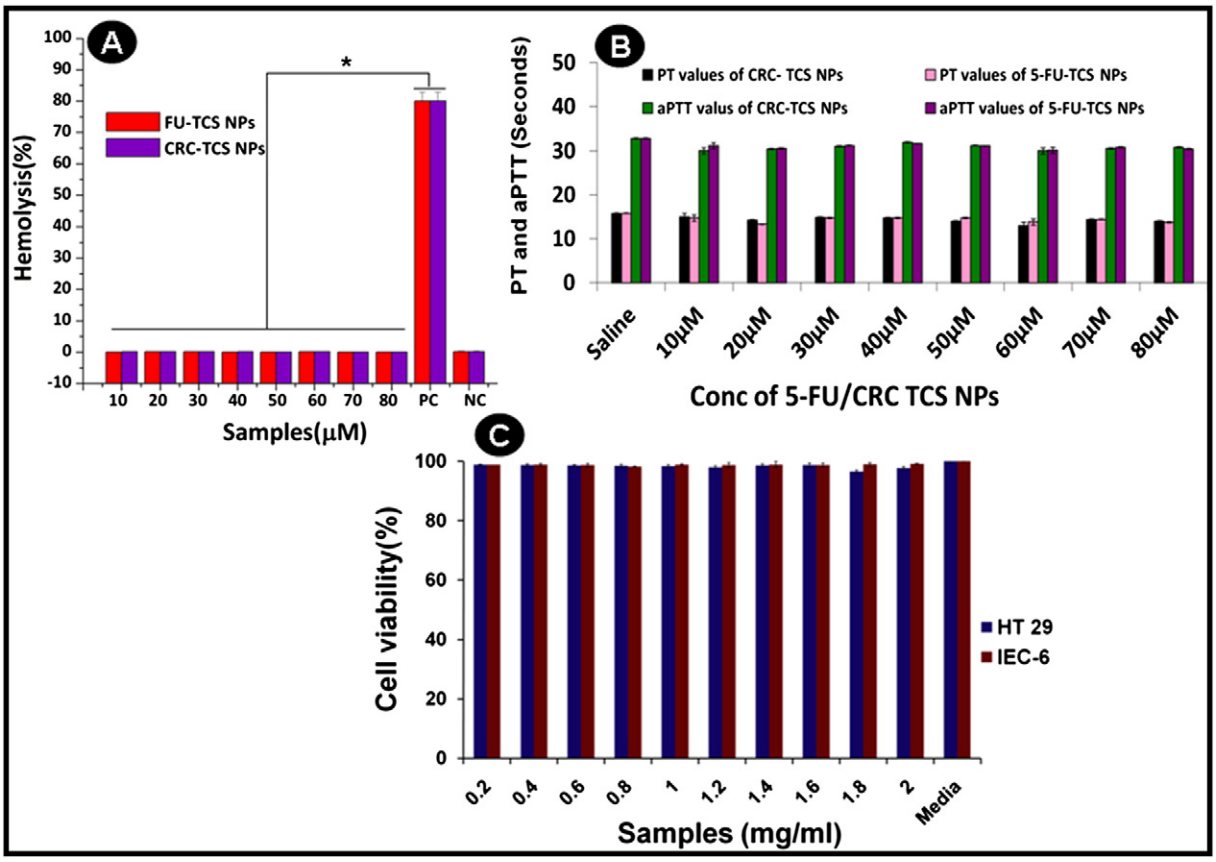

Fig. 3. (A) Hemolysis assay, (B) coagulation assay graphs, and (C) cytocompatibility of bare TCS NPs using MTT assay (48 h) (done in triplicates; n = 3, and each experiment was repeated thrice, *p < 0.05, statistical significance).

death using mitochondrial membrane potential and cell cycle analysis measurements. The detailed explanations for each of these experiments are described below.

3.8.1. Wound closure evaluation assay (scratch assay)

The wound closure results of HT29 cells after the sample treatments are shown in Fig. 5. In the figure, the percentages of wound closure of control HT29 cells and the cells treated with CRC, 5-FU, combination of bare drugs, CRC-TCS-NPs, 5-FU-TCS-NPs and combinatorial treatment were found to be 54.54 ± 3, 70 ± 1.23, 66.66 ± 2, 6.87 ± 2.5, 54.56 ± 7, 47.99 ± 10 and 5 ± 2.3% respectively. It is evident from the results that there is a significant decrease in the wound closure in cells treated with the combination nanoformulations/bare drugs than the individual nanoformulations/bare drugs.

3.8.2. MTT and live/dead assays

Fig. 6 represents the MTT assay results of CRC-TCS-NPs and 5-FU-TCS-NPs along with the control bare drugs towards IEC 6 cells. The results showed that under in vitro conditions, bare as well as drug loaded-nanoparticles showed 70–80% viability towards IEC 6 cells.

Fig. 7 represents the MTT assay results of samples treated with HT29 cells, where a, b, c, d, e, and f represents the 5-FU, CRC, combination of

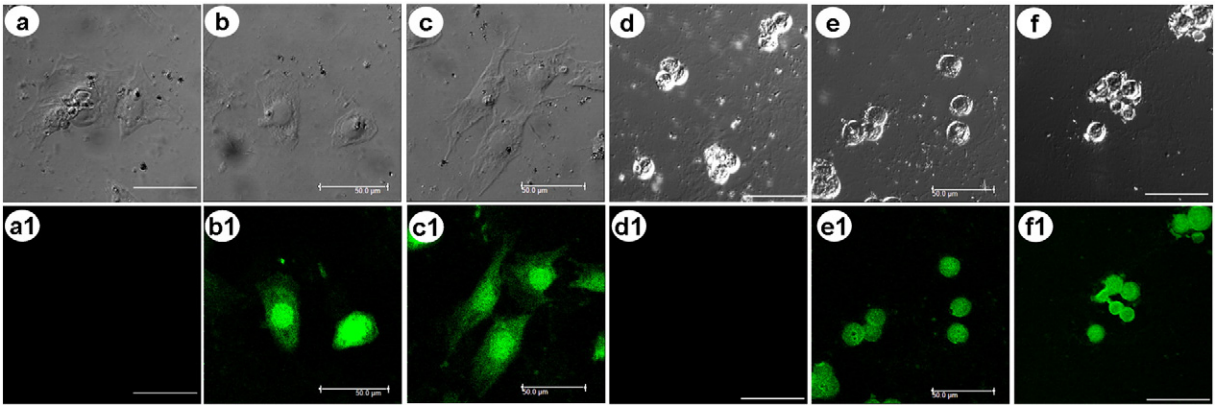

Fig. 4. Cellular uptake of Rh 123-CRC-TCS-NPs and Rh 123-5-FU-TCS-NPs using confocal imaging, where IEC 6 (a, b, c, a1, b1, c1) and HT29 (d, e, f, d1, e1, f1) cells where (a, a1) & (d, d1) represent control IEC 6 and HT29 cells, (b, b1) & (e, e1) CRC-TCS-NP treated IEC 6 and HT29 cells, (c, c1) & (f, f1) 5-FU-TCS-NP treated cells (scale bar represents 50 μm) (done in triplicates; n = 3, and each experiment was repeated thrice).

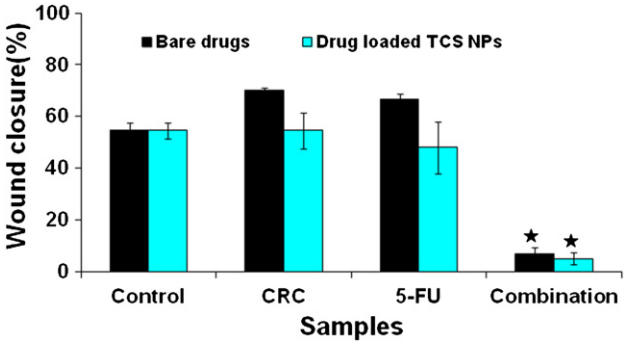

Fig. 5. Depicts the wound closure evaluation data of HT29 cells after the treatment with CRC-TCS-NPs, 5-FU-TCS-NPs, and combination of NPs in comparison with the control bare drugs after 48 h (done in triplicates; n = 3, and each experiment was repeated thrice; *p < 0.05, statistical significance).

CRC/5-FU, 5-FU-TCS-NPs, CRC-TCS-NPs, and the combination NP treated cells. From the graph it is evident that the percentages of cell death for the HT29 cells treated with samples are 24.22 ± 0.91, 32.47 ± 4.49, 86.86 ± 5.27, 24.96 ± 2.36, 37.79 ± 6.49 and 86.72 ± 0.44% respectively for 5-FU, CRC, CRC/5-FU in combination, 5-FU-TCS-NPs, CRC-TCS-NPs, and combination of both nanoparticles. From the percentage of cell death values, it is confirmed that the combinatorial anticancer effects of the drug loaded-nanoparticles and bare drugs was higher than the additive effects of the individual treatments.

In addition to MTT assay, cell death was further confirmed using live dead assay (data not shown). From the results it is proved that unlike control cells (most of the cells are viable, green fluorescence), there was cell death in cells treated with bare as well as drug loaded-nanoparticles in combination. The percentage of cell death was more in the combined treatment than with the individual drugs or drug loaded-nanoparticles.

3.8.3. Mitochondrial membrane function

The mitochondrial membrane potential measurements were carried out in HT29 cells for an incubation time of 48 h. Fig. 8A represents the flow cytometric dot plots, the regions P2 and P3 represent the red and green fluorescence which directly measure the percentage of cells with healthy and apoptotic/dead mitochondria. Fig. 8B represents the graph showing the percentage of cells with green fluorescence (percentage of apoptotic/dead cells) measured against different samples. In Fig. 8B, the percentage of cells with green fluorescence or the cells with apoptotic or dead mitochondria was found to be 31.75 ± 3.32, 18.3 ± 4.1, 72.6 ± 6.50, 31.2 ± 3.39, 17.8 ± 4.52 and

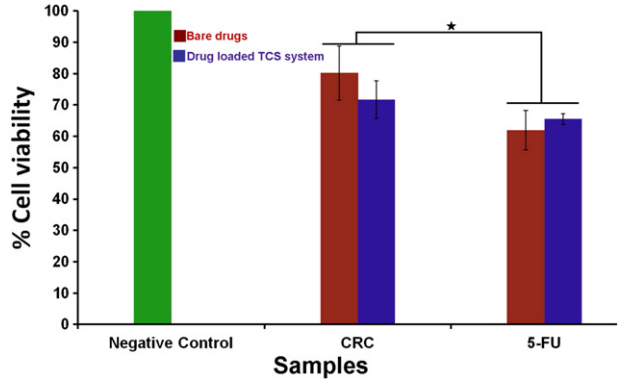

Fig. 6. Represenation of the MTT assay graphs of CRC-TCS-NPs and 5-FU-TCS-NPs along with controls towards IEC 6 cells after 48 h (done in triplicates; n = 3, and each experiment was repeated thrice, *p < 0.05, statistical significance).

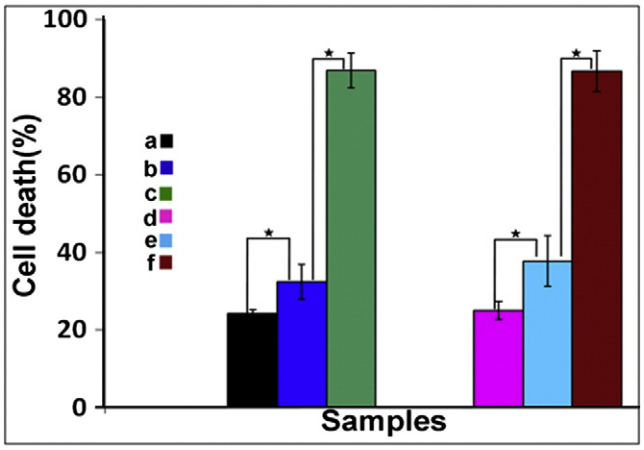

Fig. 7. Cell death analysis using MTT assay, where a, b, c, d, e, and f represent 5-FU, CRC, combination of CRC and 5-FU, 5-FU-TCS-NPs, CRC-TCS-NPs and the combination of both treated HT29 cells (48 h) (done in triplicates; n = 3, and each experiment was repeated thrice, *p < 0.05, statistical significance).

73.3 ± 10.04% respectively for the CRC, 5-FU, combination of CRC/5-FU, CRC-TCS-NPs, 5-FU-TCS-NPs, and combination of 5-FU-TCS-NPs/CRC-TCS-NPs.

3.8.4. Cell cycle analysis

Fig. 9 represents the cell cycle analysis data, where the percentage of cells in each phase was plotted against different samples, where (A), and (B) represent the data of bare and drug loaded-TCS NPs respectively. In Fig. 9A and B, the percentage of cells in the apoptotic/dead phase was found to be 27.65 ± 1.34, 23 ± 1.41, 60.8 ± 1.84, 23.8 ± 4.81, 22.95 ± 2.19, and 59.15 ± 2.33% respectively for CRC, 5-FU, CRC/5-FU in combination, CRC-TCS-NPs, 5-FU-TCS-NPs and combination of both NPs.

3.9. In vivo pharmacokinetics and biodistribution analyses in Swiss Albino mice

Fig. 10A, B, C, and D represent the pharmacokinetics and biodistribution profiles of 5-FU-TCS-NPs, CRC-TCS-NPs individually and in combination (co-administration) in Swiss Albino mice after 72 h, in comparison with the control bare drugs. The pharmacokinetic parameters derived for the CRC-TCS-NPs, 5-FU-TCS-NPs as well as the co-administered system (combination of 5-FU-TCS-NPs and CRC-TCS-NPs) and the respective bare drug solutions (data not shown) subsequent to intravenous administration are summarized in Tables 2, and 3. The plasma concentration vs. time profiles of 5-FU and CRC as in Fig. 10A and C clearly exhibit remarkable differences between the bare and drug loaded nanoformulations. The plasma 5-FU concentration–time profile of the individual (5-FU-TCS-NPs) as well as the co-administered system (combination of 5-FU-TCS-NPs and CRC-TCS-NPs) showed a peak plasma concentration; C_{max} of 56.51 ± 2.24 and 53.25 ± 6.61 μg/ml respectively at the 1st hour (t_{max}) of sample administration. The plasma concentration–time profile of 5-FU from both the individual and co-administered systems declined with time but in comparison with the bare 5-FU (data not shown, which showed a C_{max} of 69.16 ± 0.64 μg/ml within 0.25 h and declined within 12 h), the plasma concentration of 5-FU from the NPs was maintained in μg/ml quantities. Similarly the plasma CRC concentration–time profile of the individual (CRC-TCS-NPs alone) as well as the co-administered system (combination of 5-FU-TCS-NPs and CRC-TCS-NPs) showed a peak plasma concentration (C_{max}) of 18.00 ± 3.54 and 17.73 ± 2.64 μg/ml respectively at the 24th hour (t_{max}) of sample administration. The plasma concentration–time profile of CRC from both the individual and co-administered systems declined with time. But in comparison with the bare CRC

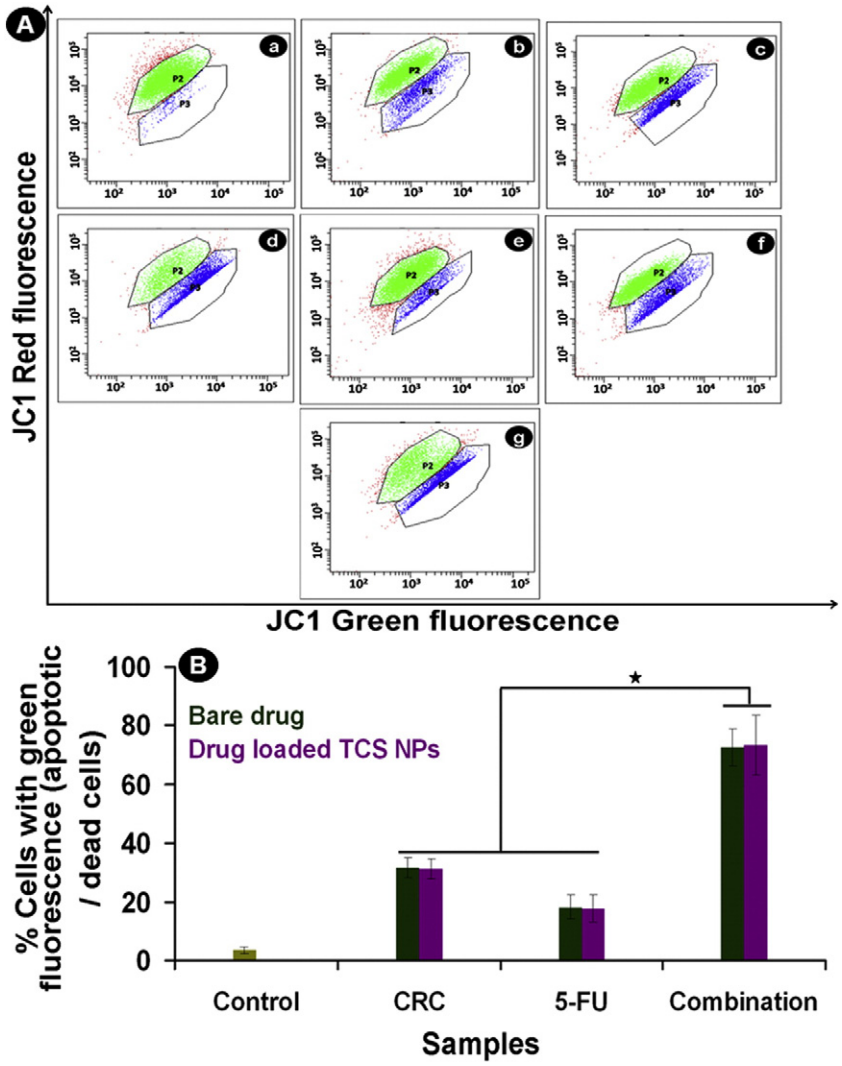

Fig. 8. (A) The flow cytometric quantification of combinatorial anticancer effects of CRC-TCS-NPs and 5-FU-TCS-NPs using mitochondrial membrane potential measurements, where (a) control HT29 cells, (b), (c), (d), (e), and (f) represent the cells treated with 5-FU, CRC, combination of 5-FU/CRC, 5-FU-TCS-NPs, CRC-TCS-NPs, and the combination of CRC-TCS-NPs/5-FU-TCS-NPs after 48 h, (B) represents the graphical representation of mitochondrial membrane potential measurements (done in triplicates; n = 3, and each experiment was repeated thrice, *p < 0.05, statistical significance).

(a peak plasma concentration of 100 ± 5.3 μg/ml was achieved at 1 h and was undetectable within the initial 6 h, data not shown) the plasma concentration of CRC from the NPs system was maintained in μg/ml quantities.

The AUC_{0-t} values of 5-FU-TCS-NPs, and 5-FU-TCS-NPs from the co-administered system were found to be 1.97 ± 0.248 and 1.65 ± 0.137 μg/ml∗h respectively which are very much greater than the AUC_{0-t} values of control (0.105 ± 0.002 μg/ml∗h). Similarly the

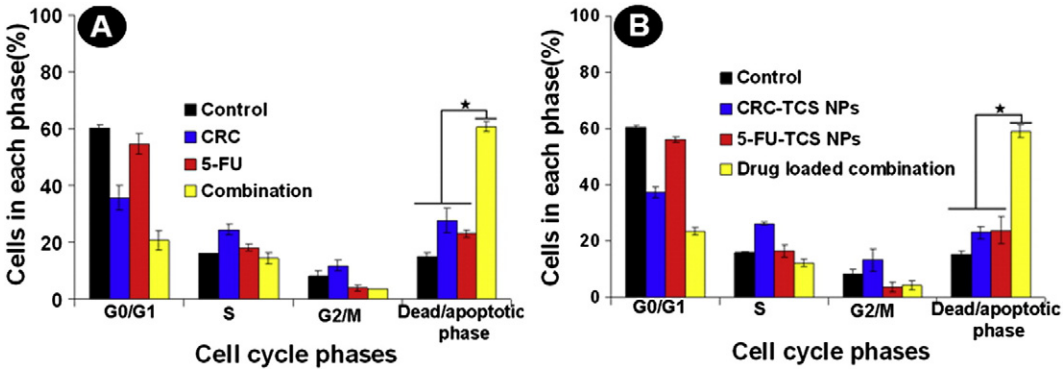

Fig. 9. (A) and (B) represent the graphical representation of the flow cytometric quantification of combinatorial anticancer effects of CRC-TCS-NPs and 5-FU-TCS-NPs using cell cycle analysis in HT29 cells after 48 h; where (A) and (B) represent the bare drugs, and drug loaded-TCS NP system respectively (done in triplicates; n = 3, and each experiment was repeated thrice, *p < 0.05, statistical significance).

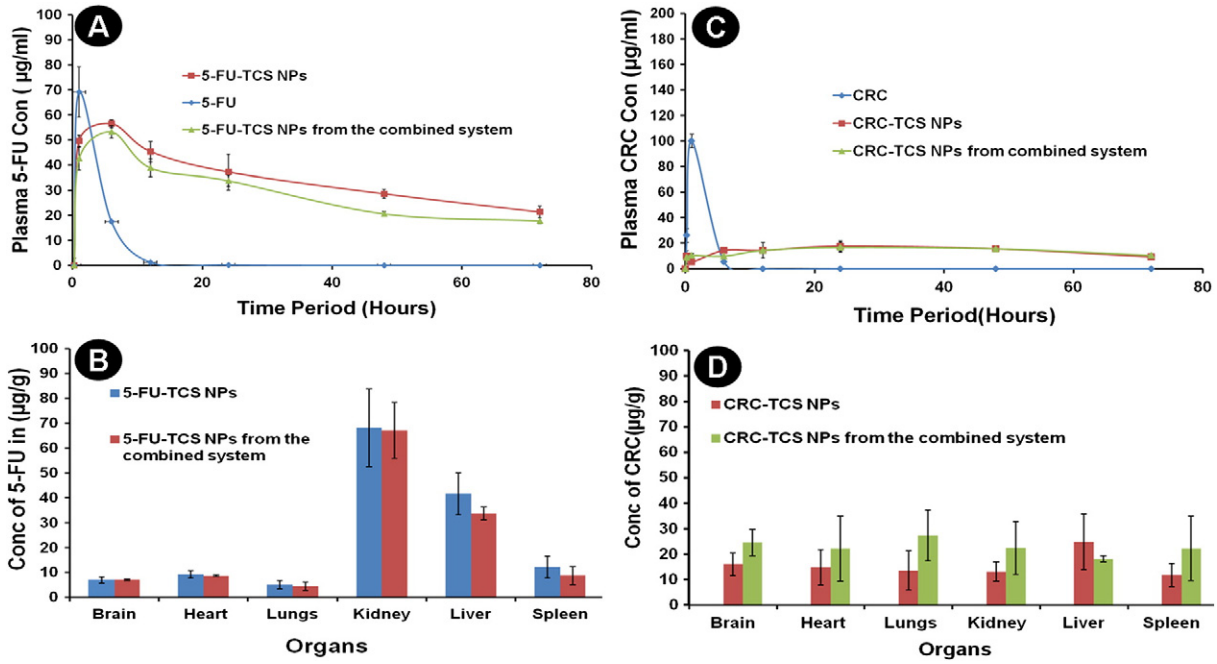

Fig. 10. (A), (B), (C) and (D) represent the pharmacokinetic and biodistribution profile of 5-FU-TCS-NPs (dose: NPs containing 20 mg/kg of 5-FU), CRC-TCS-NPs (dose: NPs containing 25 mg/kg of CRC), combination of CRC-TCS-NPs and 5-FU-TCS-NPs, bare CRC (dose: 25 mg/kg) and 5-FU (dose: 20 mg/kg) in Swiss Albino mice after 72 h, where (A) and (C) represent the pharmacokinetic profile of 5-FU-TCS-NPs and CRC-TCS-NPs, and (B) and (D) the biodistribution profile of 5-FU-TCS-NPs and CRC-TCS-NPs [intravenous administration (n = 4)].

AUC_{0-t} values of CRC-TCS-NPs, and CRC-TCS-NPs from the co-administered system were proven to have values of 1.046 ± 0.122, 1.02 ± 0.163 µg/ml∗h respectively which are also much higher than the AUC_{0-t} values of control CRC (0.158 ± 0.021 µg/ml∗h).

The pharmacokinetic parameters; V_d, $t_{1/2}$ and CL derived for the 5-FU system (5-FU-TCS-NPs and 5-FU-TCS-NPs from the combined system) and CRC system (CRC-TCS-NPs and the CRC-TCS-NPs from the combined system) is depicted in Table 3. It is very clear from the data that the pharmacokinetic parameters (V_d, $t_{1/2}$ and CL) of 5-FU and CRC were drastically modified in the NPs in comparison with the bare 5-FU and CRC (data not shown). Hence we could observe increased values of V_d, & $t_{1/2}$ and decreased values of CL for the CRC and 5-FU from the NPs in comparison with the bare drugs. Thus the $t_{1/2}$ of 5-FU from the 5-FU-TCS-NPs and 5-FU-TCS-NPs from the combined system was found to be 41.04 ± 4.96 and 63.84 ± 16.75 h respectively which is much higher than the reported $t_{1/2}$ of bare 5-FU of 15 min. The volumes of distribution; V_d values of 5-FU-TCS-NPs and 5-FU-TCS-NPs from the combined system were found to be 0.423 ± 0.03 and 0.63 ± 0.068 L respectively, which are also much higher than V_d of bare 5-FU solution (0.069 l). Similarly the CL values of 5-FU-TCS-NPs (0.007 ± 0.001 l/h) and 5-FU-TCS-NPs from the combined system (0.007 ± 0.001 l/h) were found to be far lesser than the CL values of bare 5-FU solution (0.188 ± 0.05 l/h; data not shown). Similarly for the CRC-TCS-NPs system, same trend was observed (Table 3).

The biodistribution profile of 5-FU from the individual (5-FU-TCS-NPs) as well as the co-administered system (combination of 5-FU-TCS-NPs and CRC-TCS-NPs) after 72 h is shown in Fig. 10B (the estimated 5-FU/CRC concentrations were measured in µg/g of the organs). The data clearly implies that most of the 5-FU after 72 h was detected in kidney and liver, with smaller amounts in spleen and the rest of the organs. The biodistribution pattern of CRC from the individual and co-administered system (Fig. 10(D)) was almost identical. The profile showed smaller amounts of CRC in each organ tested.

3.10. Histology studies

H and E stained tissue sections were analyzed for histopathological changes that occurred and the results are explained in Fig. 11, where Fig. 11 depicts the kidney, liver, and spleen of different tissue sections. CRC-TCS-NPs and control CRC treated samples didn't reveal any kind of inflammatory reactions (brain, heart, lungs, kidney, liver and spleen; data not shown). This is in accordance with the biodistribution data wherein small concentrations of the drug were found in these organs. For the 5-FU-TCS-NPs and the 5-FU-TCS-NP/CRC-TCS-NP groups, there were mild congestive and degenerative changes in kidney and liver. This could be due to the retention of 5-FU/5-FU-TCS-NPs in the respective organs [41].

Table 2
Pharmacokinetic parameters (t_{max}, C_{max}, and AUC_{0-t}) derived for the 5-FU-TCS-NPs, 5-FU-TCS-NPs from the combined system, CRC-TCS-NPs, and CRC-TCS-NPs from the combined system after intravenous administration in Swiss Albino mice (after 72 h).

Samples	t_{max} (h)	C_{max}	AUC_{0-t} (µg l^{-1} h^{-1})
5-FU-TCS-NPs	1	56.51 ± 2. 24	1.974 ± 0.248
5-FU-TCS-NPs from the combined system	1	53.25 ± 6.61	1.65 ± 0.137
CRC-TCS-NPs	24	18 ± 3.54	1.046 ± 0.122
CRC-TCS-NPs from the combined system	24	17.73 ± 2.64	1.023 ± 0.163

Table 3
Pharmacokinetic parameters ($t_{1/2}$, V_d, and CL) derived for the 5-FU-TCS NPs, 5-FU-TCS NPs from the combined system, CRC-TCS-NPs, and CRC-TCS-NPs from the combined system after intravenous administration in Swiss Albino mice (after 72 h).

Samples	$t_{1/2}$ (h)	V_d (l)	CL (l/h)
5-FU-TCS-NPs	41.04 ± 4.96	0.423 ± 0.03	0.007 ± 0.001
5-FU-TCS-NPs from the combined system	63.84 ± 16.75	0.63 ± 0.068	0.007 ± 0.001
CRC-TCS-NPs	49.03 ± 2.92	1.02 ± 0.07	0.0095 ± 0.008
CRC-TCS-NPs from the combined system	61.27 ± 11.91	1.07 ± 0.22	0.008 ± 0.007

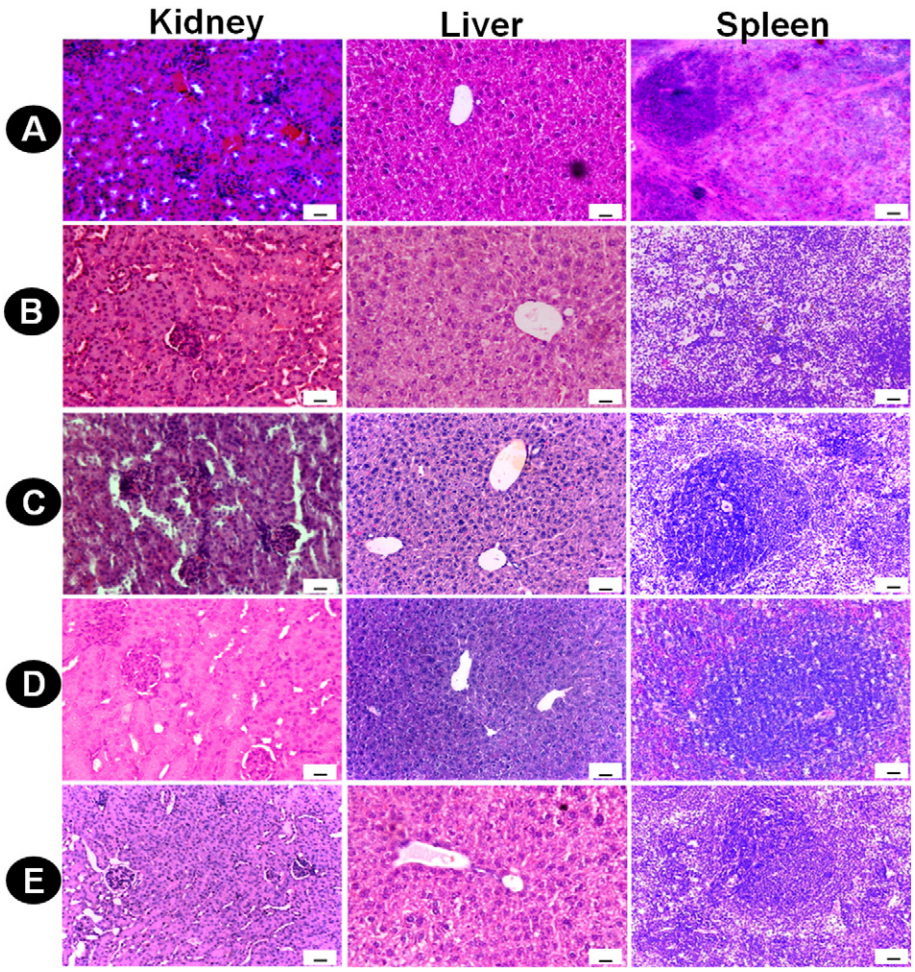

Fig. 11. The optical images of H and E stained organs of mice (kidney, liver and spleen) after 72 h, where (A) saline, (B) combination of bare drugs, (C) 5-FU-TCS-NPs,(D) CRC-TCS-NPs, and (E) combination of 5-FU-TCS-NPs/CRC-TCS-NPs (scale bar represents 20 μm) (n = 4).

4. Discussion

Stable CRC-TCS-NPs and 5-FU-TCS-NPs of spherical shape and size of about 150 ± 50 nm were developed by TPP cross-linking [30,32]. The drug entrapment results from the ionic interaction/hydrogen bonding between TCS, TPP, and CRC (for CRC-TCS-NPs) and TCS, TPP, and 5-FU (for 5-FU-TCS-NPs) which can be explained well with the help of FT-IR. The EE for the CRC-TCS-NPs was higher than the 5-FU-TCS-NP system and decremented EE in the latter results from the hydrophilicity of 5-FU. The in vitro drug release mechanism can be explained as follows, the initial burst release is the result of surface adsorbed drug and the sustained pattern happens as a result of the slow degradation of the carrier TCS system. The degradation of TCS NPs occurs through hydrolysis reaction, where the glucosamine–glucosamine, glucosamine–*N*-acetyl glucosamine and *N*-acetyl glucosamine–*N*-acetyl glucosamine linkages are disrupted, ultimately resulting in an incremented release. The enhanced drug release in acidic pH results from the acid dependent swelling followed by degradation of the carrier matrix [32,51–53]. The hemocompatibility of 5-FU-TCS-NPs and CRC-TCS-NPs was confirmed by different assays. The percentage of hemolysis was below 5%, which is the critical limit for a biomaterial to be used for intravenous administration applications [31,54]. The coagulation time, PT and aPTT values remain in the normal range, which further confirmed hemocompatibility. For any biomaterial to be utilized for preclinical and clinical evaluation, hemocompatibility is a key requisite [55]. The cytocompatibility of TCS-NPs for a range of concentration from 0.2 to 2 mg/ml was also confirmed. Confocal imaging substantiated the cellular internalization of Rh 123-5-FU-TCS-NPs and Rh 123-CRC-TCS-NPs in IEC 6 and HT29 cells. Since the nanoparticles were positively charged and had sizes below 200 nm, the uptake happens through pino- or macropinocytosis [56]. In clinical or preclinical perspective, the current system is passively targeted, the EPR effect of the tumor microenvironment results in enhanced uptake of the nanoparticles in cancer cells unlike in normal cells [56].

The in vitro combinatorial anticancer effects of the nanoformulations were proven by different assays in HT29 cells. The MTT and live/dead assay results proved the enhanced anticancer effects unlike the individual nanoformulations. Further these results were confirmed by mitochondrial membrane potential and cell cycle analysis. Thus the MTT, live/dead, and the mitochondrial membrane potential results were well in correlation with the cell cycle analysis data, where a significant percentage of apoptosis/cell death was proven in combinatorial treatment.

CRC and 5-FU individually induces colon cancer cell death by apoptosis through the arrest of cells in the G2/M and S phase respectively. Therefore we could see a small percentage of cells which accumulated in the P6 phase (apoptotic) of cells treated with the individual nanoparticles and bare drugs. Whereas in combination, the anticancer effects were enhanced, thus we could get apoptosis percentage of 60.8 ± 1.84, and 59.15 ± 2.33% respectively for the 5-FU/CRC in combination, and combination of CRC-TCS-NPs and 5-FU-TCS-NPs.

CRC induces p53-mediated apoptosis through two sets of genes upon stress signals, p21/waf1 and GADD45. The main functions of these genes involve the cell growth control, and the latter acting on

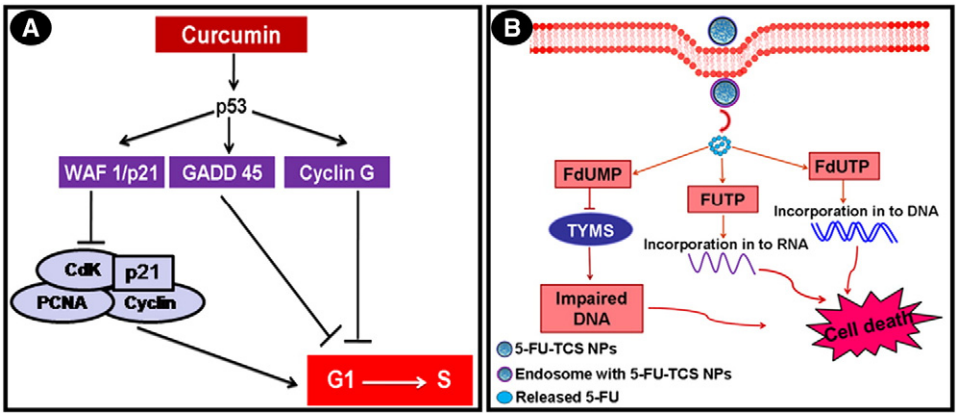

Fig. 12. (A) Represents the mechanism of CRC induced anticancer effects in HT29 cells, and (B) pathway representing the mechanism of 5-FU induced anticancer effects in HT29 cells.

Bax leading to apoptosis [57]. The diagrammatic representation of p53 mediated cell cycle regulation is shown in Fig. 12A. p53 induces the expression of different cell cycle regulating proteins, p21 (encoded by the Waf 1). This in turn inactivates the formation of cyclin dependent kinase (Cdk)–cyclin complex leading to the arrest of cells in the G1-S phase [55]. The cytotoxic metabolites of 5-FU; fluorodeoxyuridine monophosphate (FdUMP), fluoro-deoxyuridine triphosphate (FdUTP) and fluorouridine triphosphate (FUTP) are incorporated into the DNA and RNA causing cell cycle arrest which in turn results in apoptosis (Fig. 12B). FdUMP can also inhibit thymidylate synthase (TYMS) enzyme, thereby blocking the synthesis of pyrimidine thymidine, which is required for DNA replication [47,48]. Thus the CRC introduction in colon cancer cells results in the down regulation of COX-2 mRNA/protein expression, which in turn improves the anticancer efficacy of 5-FU [13,14].

The pharmacokinetic results proved that the entrapment of 5-FU/CRC in TCS NPs improved the plasma concentration–time profile of 5-FU and CRC. The plasma concentration–time profiles of the co-administered systems were matched with the individual administrations. This has been proven by evaluating the AUC_{0-t} values of individual as well as the co-administered system. There was no significant difference in the AUC_{0-t} values (Table 2) of the individual and the combined (co-administered) systems. The increased AUC_{0-t} values of the 5-FU and CRC nanoparticle systems indicate an enhanced bioavailability of both drugs, which was not achievable with the bare drug solutions.

Thus our experimental results showed that the 5-FU-TCS-NPs and CRC-TCS-NPs could circulate in the blood at a higher level for 3 days implying its improved systemic retention in the circulation. Also the C_{max} of 5-FU and CRC are lower in plasma and AUC was higher than the control bare drugs. It indicates that the 5-FU and CRC which are entrapped in the TCS nanoparticles, was slowly released into the blood with the slow degrdation of carrying TCS nanoparticles, thereby improving the bioavailability of 5-FU and CRC. This is clearly evident from the improved pharmacokinetic parameters (ie, the improved $t_{1/2}$, V_d, AUC_{0-t} and deceased CL) of CRC and 5-FU from the nanoformulation in comparison with the control drugs. Our results on the improved bioavailability of CRC and 5-FU correlated well with the reported literatures [3,5,23,35,37,58–65]. In addition, the in vivo pharmacokinetic results of CRC-TCS-NPs, 5-FU-TCS-NPs individually and in combination revealed 28.6 ± 7.07 and 14.27 ± 4.00 μg/ml quantities of 5-FU and CRC, respectively, in plasma up to 72 h. The plasma concentration of 5-FU from a block copolymer was reported earlier, and it showed 40–60 μg/ml of 5-FU up to 48 h. The system was proven to be inhibiting the growth of colon cancer xenograft model [3]. In the current experiment, the plasma 5-FU/CRC concentration from the NP systems comes in the range where the in vitro combinatorial anticancer effects were proven.

The biodistribution data of 5-FU from the individual as well as the combination system is comparable with the reported literature, where Yan et al. had proved the retention of 5-FU-NPs in different tissues as in the following order; liver > kidney > spleen after the intravenous administration of 30 mg/kg of 5-FU–succinyl chitosan nanoparticles [5,66,67]. Here in our study also, the distribution pattern showed smaller fractions of 5-FU in each organ tested in the following order; kidney > liver > spleen > brain = heart = lungs. The higher retention of 5-FU in the kidney may be due to the hydrophilicity of 5-FU which is eliminated through the kidney. The retention of 5-FU in liver and spleen may be due to the highly perfused nature of these organs [5,66,67]. The CRC distribution in liver may be due to the drug metabolism and hepatic elimination, and in kidney, due to the renal clearance [26]. The distribution in spleen and lungs may be related to the phagocytosis process by the respective macrophages in those organs [26,68]. The CRC retention in lungs may be attributed to the filtration of pulmonary capillary beds following intravenous injection of the nanoparticles [26]. The small quantities in brain may be the result of blood–brain barrier penetration of hydrophobic CRC [26,69]. The highly perfused nature of the heart may be the reason for the retention of CRC in the heart [26].

The study needs to be extended to analyze and prove the in vivo synergistic anticancer effects of 5-FU-TCS-NPs in combination with CRC-TCS-NPs in colon cancer xenograft model. Further if the tumor reduction results are promising, the current systems of 5-FU/CRC in TCS NPs could be utilized as a combinatorial nanomedicine against colon cancer, in which the efficacy of 5-FU as a chemo drug could be enhanced and the dose reduction can be achieved [3]. H and E analysis confirmed the nontoxic nature of CRC/CRC-TCS-NPs after 72 h, where as the 5-FU/5-FU-TCS-NPs showed mild congestive and degenerative changes in kidney and liver that results from the accumulation of 5-FU-TCS-NPs in kidney and liver [70].

5. Conclusions

The nanoformulations of CRC and 5-FU were developed in TCS to overcome the drawbacks of 5-FU and CRC. The developed NPs were about 150 ± 50 nm in size with high colloidal stability and blood compatibility. The in vitro studies proved the enhanced anticancer effects (2.5 to 3 fold) of combined treatment in comparison with the individual and control bare drugs. The in vivo studies proved the improved plasma half life of nanoentrapped 5-FU and the CRC up to 72 h. The biodistribution data confirmed the accumulation of 5-FU-TCS-NPs in liver and small portions in kidney and spleen. For the CRC-TCS-NPs, small quantities of CRC in the different organs tested were found. However in future, the tumor reduction studies in colon cancer xenograft model needs to be analyzed strictly to prove the synergistic anticancer effects of drug loaded-NPs (CRC-TCS-NPs with 5-FU-TCS-NPs) and to translate the nanomediucine in to the clinical side.

Acknowledgements

The authors are thankful to the Department of Biotechnology (DBT), Government of India, for their financial support for this work under the Nanoscience and Nanotechnology Initiative program (Ref. No. BT/PR10882/NNT/28/142/2008). The authors are thankful to the Department of Science and Technology (DST) under the project 'Nanotheragnostics' (SR/NM/NS-99/2009) for funding the work. The authors are thankful to Dr. A. K. K. Unni, Dr. Reshmi P, Dr. Sahadev Shankarappa and Miss Shanthini for their immense help in the animal experiments and histopathology studies. One of the authors, A. Anitha, is thankful to the Council of Scientific and Industrial Research (CSIR), India for providing Senior Research Fellowship (SRF award—Ref. No. 9/963 (0005) 2K10-EMR-I) for carrying out her research work. The authors are also thankful to Koyo Chemicals Co. Ltd., Japan for providing chitosan. The authors are also thankful to Mr. Sajin P. Ravi, Mr. Sarath, Mrs. P R Sreerekha, Mr. Sunil, Mr. Sajith and Mrs. Sunitha for their help in SEM, confocal microscopy, flow cytometry and in vivo experiments.

References

[1] P. Pisani, D.M. Parkin, J. Ferlay, Estimates of the worldwide mortality from eighteen major cancers in 1985. Implications for prevention and projections of future burden, Int. J. Cancer 55 (1993) 891–903.
[2] K. Sakamoto, M. Shin, Targeting NF-κB for colorectal cancer, Expert Opin. Ther. Targets 14 (2010) 593–601.
[3] S. Li, A. Wang, W. Jiang, Z. Guan, Pharmacokinetic characteristics and anticancer effects of 5-fluorouracil loaded nanoparticles, BMC Cancer 15 (2008) 103–111.
[4] R. Ortiz, J. Prados, C. Melguizo, J.L. Arias, M.A. Ruiz, P.J. Alvarez, O. Caba, R. Luque, A. Segura, A. Aranega, 5-Fluorouracil-loaded poly(ε-caprolactone) nanoparticles combined with phage E gene therapy as a new strategy against colon cancer, Int. J. Nanomedicine 7 (2012) 95–107.
[5] C. Yan, J. Gu, Y. Guo, D. Chen, In vivo biodistribution for tumor targeting of 5-fluorouracil loaded *N*-succinyl chitosan nanoparticles, Pharm. Soc. Jpn. 130 (2010) 801–804.
[6] Y. Zhang, J. Li, M. Lang, X. Tang, L. Li, X. Shen, Folate-functionalized nanoparticles for controlled 5-fluorouracil delivery, J. Colloid Interface Sci. 354 (2011) 202–209.
[7] A. de Gramont, A. Figer, M. Seymour, M. Homerin, A. Hmissi, J. Cassidy, C. Boni, H. Cortes-Funes, A. Cervantes, G. Freyer, D. Papamichael, N. Le Bail, C. Louvet, D. Hendler, F. de Braud, C. Wilson, F. Morvan, A. Bonetti, Leucovorin and fluorouracil with or without oxaliplatin as first-line treatment in advanced colorectal cancer, J. Clin. Oncol. 18 (2000) 2938–2947.
[8] R.B. Diasio, M.R. Johnson, The role of pharmacogenetics and pharmacogenomics in cancer chemotherapy with 5-fluorouracil, Pharmacology 61 (2000) 199–203.
[9] J. Viguier, V. Boige, C. Miquel, M. Pocard, B. Giraudeau, J.C. Sabourin, M. Ducreux, A. Sarasin, F. Praz, ERCC1 codon 118 polymorphism is a predictive factor for the tumor response to oxaliplatin/5-fluorouracil combination chemotherapy in patients with advanced colorectal cancer, Clin. Cancer Res. 11 (2005) 6212–6217.
[10] J. Guo, A.W. Zhou, Y.C. Fu, U.N. Verma, D. Tripathy, E.P. Frenkel, C.R. Becerra, Efficacy of sequential treatment of HCT116 colon cancer monolayers and xenografts with docetaxel, flavopiridol, and 5-fluorouracil, Acta Pharmacol. Sin. 27 (2006) 1375–1381.
[11] J.T. Hwang, J. Ha, O.J. Park, Combination of 5-fluorouracil and genistein induces apoptosis synergistically in chemo resistant cancer cells through the modulation of AMPK and COX-2 signaling pathways, Biochem. Biophys. Res. Commun. 332 (2005) 433–440.
[12] S. Carnesecchi, R. Bras-Goncalves, A. Bradaia, M. Zeisel, F. Gosse, M.F. Poupon, F. Raul, Geraniol, a component of plant essential oils, modulates DNA synthesis and potentiates 5-fluorouracil efficacy on human colon tumor xenografts, Cancer Lett. 215 (1) (2004) 53–59.
[13] B. Du, L. Jiang, Q. Xia, L. Zhong, Synergistic inhibitory effects of curcumin and 5-fluorouracil on the growth of the human colon cancer cell line HT-29, Chemotherapy 52 (2006) 23–28.
[14] K. Srimuangwong, C. Tocharus, J. Tocharus, A. Suksamrarn, P.Y. Chintana, Effects of hexahydrocurcumin in combination with 5-fluorouracil on dimethylhydrazine-induced colon cancer in rats, World J. Gastroenterol. 18 (2012) 6951–6959.
[15] M. Sun, Z. Estrov, Y. Ji, K.R. Coombes, D.H. Harris, R. Kurzrock, Curcumin (diferuloylmethane) alters the expression profiles of microRNAs in human pancreatic cancer cells, Mol. Cancer Ther. 7 (2008) 464–473.
[16] N. Dhillon, B.B. Aggarwal, R.A. Newman, R.A. Wolff, A.B. Kunnumakkara, J.L. Abbruzzese, C.S. Ng, V. Badmaev, R. Kurzrock, Phase II trial of curcumin in patients with advanced pancreatic cancer, Clin. Cancer Res. 14 (2008) 4491–4499.
[17] K. Nakamura, Y. Yasunaga, T. Segawa, D. Ko, J.W. Moul, S. Srivastava, J.S. Rhim, Curcumin down-regulates AR gene expression and activation in prostate cancer cell lines, Int. J. Oncol. 21 (2002) 825–830.
[18] S.H. Wu, L.W. Hang, J.S. Yang, H.Y. Chen, H.Y. Lin, J.H. Chiang, C.C. Lu, J.L. Yang, T.Y. Lai, Y.C. Ko, J.G. Chung, Curcumin induces apoptosis in human non-small cell lung cancer NCI-H460 cells through ER stress and caspase cascade- and mitochondria-dependent pathways, Anticancer Res. 30 (2010) 2125–2134.
[19] J.J. Jeremy, M. Hasan, Curcumin for chemoprevention of colon cancer, Cancer Lett. 255 (2) (2007) 170–181.
[20] C.C. Su, J.G. Lin, T.M. Li, J.G. Chung, J.S. Yang, S.W. Ip, W.C. Lin, G.W. Chen, Curcumin-induced apoptosis of human colon cancer colo 205 cells through the production of ROS, Ca^{2+} and the activation of caspase-3, Anticancer Res. 26 (2006) 4379–4389.
[21] R. Hanif, L. Qiao, S.J. Shiff, B. Rigas, Curcumin, a natural plant phenolic food additive, inhibits cell proliferation and induces cell cycle changes in colon adenocarcinoma cell lines by a prostaglandin-independent pathway, J. Lab. Clin. Med. 130 (1997) 576–584.
[22] C.R. Ireson, D.J. Jones, S. Orr, M.W. Coughtrie, D.J. Boocock, M.L. Williams, P.B. Farmer, W.P. Steward, A.J. Gescher, Metabolism of the cancer chemopreventive agent curcumin in human and rat intestine, Cancer Epidemiol. Biomarkers Prev. 11 (2002) 105–111.
[23] J. Shaikh, D.D. Ankola, V. Beniwal, D. Singh, M.N. Kumar, Nanoparticle encapsulation improves oral bioavailability of curcumin by at least 9-fold when compared to curcumin administered with piperine as absorption enhancer, Eur. J. Pharm. Sci. 37 (2009) 223–230.
[24] V. Kakkar, S. Singh, D. Singla, I.P. Kaur, Exploring solid lipid nanoparticles to enhance the oral bioavailability of curcumin, Mol. Nutr. Food Res. 55 (2011) 495–503.
[25] S. Acharya, S.K. Sahoo, PLGA nanoparticles containing various anticancer agents and tumour delivery by EPR effect, Adv. Drug Deliv. Rev. 63 (2011) 170–183.
[26] Y.M. Tsai, C.F. Chien, L.C. Lin, T.H. Tsai, Curcumin and its nano-formulation: the kinetics of tissue distribution and blood–brain barrier penetration, Int. J. Pharm. 416 (2011) 331–338.
[27] M.M. Yallapu, M. Jaggi, S.C. Chauhan, Curcumin nanoformulations: a future nanomedicine for cancer, Drug Discov. Today 17 (2012) 71–80.
[28] K. Srimuangwong, C. Tocharus, P.Y. Chintana, A. Suksamrarn, J. Tocharus, Hexahydrocurcumin enhances inhibitory effect of 5-fluorouracil on HT-29 human colon cancer cells, World J. Gastroenterol. 18 (2012) 2383–2389.
[29] A. Bernkop-Schnurch, M. Hornof, T. Zoidl, Thiolated polymers–thiomers: synthesis and in vitro evaluation of chitosan-2-iminothiolane conjugates, Int. J. Pharm. 260 (2003) 229–237.
[30] A. Anitha, N. Deepa, K.P. Chennazhi, S.V. Nair, H. Tamura, R. Jayakumar, Development of mucoadhesive thiolated chitosan nanoparticles for biomedical applications, Carbohydr. Polym. 83 (2011) 66–73.
[31] A. Anitha, S. Maya, N. Deepa, K.P. Chennazhi, S.V. Nair, R. Jayakumar, Curcumin-loaded *N,O*-carboxymethyl chitosan nanoparticles for cancer drug delivery, J. Biomater. Sci. Polym. Ed. 23 (2012) 1381–1400.
[32] A. Anitha, K.P. Chennazhi, S.V. Nair, R. Jayakumar, 5-Flourouracil loaded *N,O*-carboxymethyl chitosan nanoparticles as an anticancer nanomedicine for breast cancer, J. Biomed. Nanotechnol. 8 (2012) 29–42.
[33] B. Kubista, K. Trieb, F. Sevelda, C. Toma, F. Arrich, P. Heffeter, L. Elbling, H. Sutterluty, K. Scotlandi, R. Kotz, M. Micksche, W. Berger, Anticancer effects of zoledronic acid against human osteosarcoma cells, J. Orthop. Res. 24 (2006) 1145–1152.
[34] S.J. Choi, J.M. Oh, J.H. Choy, Biocompatible nanoparticles intercalated with anticancer drug for target delivery: pharmacokinetic and biodistribution study, J. Nanosci. Nanotechnol. 10 (2010) 2913–2916.
[35] P. Anand, H.B. Nair, B. Sung, A.B. Kunnumakkara, V.R. Yadav, R.R. Tekmal, B.B. Aggarwal, Design of curcumin-loaded PLGA nanoparticles formulation with enhanced cellular uptake, and increased bioactivity in vitro and superior bioavailability in vivo, Biochem. Pharmacol. 79 (2010) 330–338.
[36] Z. Ma, A. Shayeganpour, D.R. Brocks, A. Lavasanifar, J. Samuel, High-performance liquid chromatography analysis of curcumin in rat plasma: application to pharmacokinetics of polymeric micellar formulation of curcumin, Biomed. Chromatogr. 21 (2007) 546–552.
[37] Z. Song, R. Feng, M. Sun, C. Guo, Y. Gao, L. Li, G. Zhai, Curcumin-loaded PLGA–PEG–PLGA triblock copolymeric micelles: preparation, pharmacokinetics and distribution in vivo, J. Colloid Interface Sci. 354 (2011) 116–123.
[38] G.A. Shabir, Validation of high-performance liquid chromatography methods for pharmaceutical analysis: understanding the differences and similarities between validation requirements of the US Food and Drug Administration, the US Pharmacopeia and the International Conference on Harmonization, J. Chromatogr. A 987 (2003) 57–66.
[39] K.T. Smitha, A. Anitha, T. Furuike, H. Tamura, S.V. Nair, R. Jayakumar, In vitro evaluation of paclitaxel loaded amorphous chitin nanoparticles for colon cancer drug delivery, Colloids Surf. B 104 (2013) 245–253.
[40] K. Manjunath, V. Venkateswarlu, Pharmacokinetics, tissue distribution and bioavailability of clozapine solid lipid nanoparticles after intravenous and intraduodenal administration, J. Control. Release 107 (2005) 215–228.
[41] C. Alexiou, W. Arnold, P. Hulin, R.J. Klein, H. Renz, F.G. Parak, C. Bergemann, A.S. Lubbe, Magnetic mitoxantrone nanoparticle detection by histology, X-ray and MRI after magnetic tumor targeting, J. Magn. Magn. Mater. 225 (2001) 187–193.
[42] P. Huang, Z. Li, H. Hu, D. Cui, Synthesis and characterization of bovine serum albumin-conjugated copper sulfide nanocomposites, Journal of Nanomaterials, Hindawi Publishing Corporation, 2010, http://dx.doi.org/10.1155/2010/641545.
[43] A. Anitha, V.V. Divya Rani, R. Krishna, V.N. Sreeja, N. Selvamurugan, S.V. Nair, H. Tamura, R. Jayakumar, Synthesis, characterization, cytotoxicity and antibacterial studies of chitosan, *O*-carboxymethyl and *N,O*-carboxymethyl chitosan nanoparticles, Carbohydr. Polym. 78 (2009) 672–677.
[44] R.B. Devika, B.P. Varsha, Studies on effect of pH on cross-linking of chitosan with sodium tripolyphosphate: a technical note, AAPS Pharm. Sci. Technol. 7 (2006) 1–6.
[45] N.S. Rejinold, M. Muthunarayanan, K. Muthuchelian, K.P. Chennazhi, S.V. Nair, R. Jayakumar, Saponin-loaded chitosan nanoparticles and their cytotoxicity to cancer cell lines in vitro, Carbohydr. Polym. 84 (2011) 407–416.

[46] E.B. Yassin, M.K. Anwer, H.A. Mowafy, I.M. Elbagory, M.A. Bayomi, I.A. Alsarra, Optimization of 5-fluorouracil solid-lipid nanoparticles: a preliminary study to treat colon cancer, Int. J. Med. Sci. 7 (2010) 398–408.
[47] N.S. Rejinold, K.P. Chennazhi, S.V. Nair, H. Tamura, R. Jayakumar, Biodegradable and thermo-sensitive chitosan-*g*-poly (*N*-vinylcaprolactam) nanoparticles as a 5-fluorouracil carrier, Carbohydr. Polym. 83 (2011) 776–786.
[48] D. Yan, C. Chen, J. Gu, J. Qin, Nanoparticles of 5-fluorouracil (5-FU) loaded N-succinyl–chitosan (Suc–Chi) for cancer chemotherapy: preparation, characterization — in vitro drug release and antitumour activity, J. Pharm. Pharmacol. 58 (2006) 1177–1186.
[49] S. Bisht, G. Feldmann, S. Soni, R. Ravi, C. Karikar, A. Maitra, A. Maitra, Polymeric nanoparticle-encapsulated curcumin ("nanocurcumin"): a novel strategy for human cancer therapy, J. Nanobiotechnol. 5 (2007) 3, http://dx.doi.org/10.1186/1477-3155-5-3.
[50] M.M. Yallapu, M. Jaggi, S.C. Chauhan, beta-Cyclodextrin-curcumin self-assembly enhances curcumin delivery in prostate cancer cells, Colloids Surf. B 79 (2010) 113–125.
[51] T. Kean, M. Thanou, Biodegradation, biodistribution and toxicity of chitosan, Adv. Drug Deliv. Rev. 62 (2010) 3–11.
[52] S.A. Agnihotri, N.N. Mallikarjuna, T.M. Aminabhavi, Recent advances on chitosan-based micro- and nanoparticles in drug delivery, J. Control. Release 100 (2004) 5–28.
[53] I. Aranaz, M. Mengíbar, R. Harris, I. Panos, B. Miralles, N. Acosta, G. Galed, A. Heras, Functional characterization of chitin and chitosan, Curr. Chem. Biol. 3 (2009) 203–230.
[54] F.M. Gutierrez, E.P. Thi, J.M. Silverman, C.C. de Oliveira, S.L. Svensson, A.V. Hoek, E.M. Sanchez, N.E. Reiner, E.C. Gaynor, E.L.G. Pryzdial, E.M. Conway, E. Orrantia, F. Ruiz, Y. Av-Gay, H. Bach, Antibacterial activity, inflammatory response, coagulation and cytotoxicity effects of silver nanoparticles, Nanomed. Nanotechnol. Biol. Med. 8 (2012) 328–336.
[55] J.M. Koziara, J.J. Oh, W.S. Akers, S.P. Ferraris, R.J. Mumper, Blood compatibility of cetyl alcohol/polysorbate-based nanoparticles, Pharm. Res. 22 (2005) 1821–1828.
[56] B. Yu, Y. Zhang, W. Zheng, C. Fan, T. Chen, Positive surface charge enhances selective cellular uptake and anticancer efficacy of selenium nanoparticles, Inorg. Chem. 51 (2012) 8956–8963.
[57] M.L. Agarwal, W.R. Taylor, M.V. Chernov, O.B. Chernova, G.R. Stark, The p53 network, J. Biol. Chem. 273 (1998) 1–4.
[58] M. Cheng, H. Chen, Y. Wang, H. Xu, B. He, J. Han, Z. Zhang, Optimized synthesis of glycyrrhetinic acid-modified chitosan 5-fluorouracil nanoparticles and their characteristics, Int. J. Nanomedicine 24 (2014) 695–710.
[59] M.R. Cheng, Q. Li, T. Wan, B. He, J. Han, H.-X. Chen, F.-X. Yang, W. Wang, H.-Z. Xu, T. Ye, B-B. Zha, Galactosylated chitosan/5-fluorouracil nanoparticles inhibit mouse hepatic cancer growth and its side effects, World J. Gastroenterol. 18 (2012) 6076–6087.
[60] N.M. Khalil, T.C.F. do Nascimento, D.M. Casa, L.F. Dalmolin, A.C. deMattos, I. Hoss, Pharmacokinetics of curcumin-loaded PLGA and PLGA–PEG blend nanoparticles after oral administration in rats, Colloids Surf. B 101 (2013) 353–360.
[61] R. Feng, Z. Song, G. Zhai, Preparation and in vivo pharmacokinetics of curcumin-loaded PCL–PEG–PCL triblock copolymeric nanoparticles, Int. J. Nanomedicine 7 (2012) 4089–4098.
[62] L. Zhongfa, M. Chiu, J. Wang, W. Chen, W. Yen, P. Fan-Havard, Enhancement of curcumin oral absorption and pharmacokinetics of curcuminoids and curcumin metabolites in mice, Cancer Chemother. Pharmacol. 69 (2012) 679–689.
[63] S. Jiabei, B. Chao, M.C. Hok, S. Shaoping, Z. Qingwen, Z. Ying, Curcumin-loaded solid lipid nanoparticles have prolonged in vitro antitumour activity, cellular uptake and improved in vivo bioavailability, Colloids Surf. B 111 (2013) 367–375.
[64] A.A. Ghahremankhani, F. Dorkoosh, R. Dinarvand, PLGA–PEG–PLGA tri-block copolymers as in situ gel-forming peptide delivery system: effect of formulation properties on peptide release, Pharm. Dev. Technol. 13 (2008) 49–55.
[65] A.M. Thomas, A.I. Kapanen, J.I. Hare, E. Ramsay, K. Edwards, G. Karlsson, M.B. Bally, Development of a liposomal nanoparticle formulation of 5-fluorouracil for parenteral administration: formulation design, pharmacokinetics and efficacy, J. Control. Release 150 (2011) 212–219.
[66] S. Schmidt, D. Gonzalez, H. Derendorf, Significance of protein binding in pharmacokinetics and pharmacodynamics, J. Pharm. Sci. 99 (2010) 1107–1122.
[67] D.H. Ho, L. Townsend, M.A. Luna, G.P. Bodey, Distribution and inhibition of dihydrouracil dehydrogenase activities in human tissues using 5-fluorouracil as a substrate, Anticancer Res. 6 (1986) 781–784.
[68] S.M. Moghimi, A.C. Hunter, J.C. Murray, Long-circulating and target-specific nanoparticles: theory to practice, Pharmacol. Rev. 53 (2001) 283–318.
[69] T.G. Park, Degradation of poly(lactic-co-glycolic acid) microspheres: effect of copolymer composition, Biomaterials 16 (1995) 1123–1130.
[70] P.D. King, M.C. Perry, Hepatotoxicity of chemotherapy, Oncologist 6 (2001) 162–176.